

Characterization of offline analysis of particulate matter with FIGAERO-CIMS

Jing Cai^{1,2,#}, Kaspar R. Daellenbach^{1,2,3,#,*}, Cheng Wu^{4,5}, Yan Zheng⁶, Feixue Zheng¹, Wei Du^{1,2}, Sophie L. Haslett⁴, Qi Chen⁶, Markku Kulmala^{1,2}, Claudia Mohr^{4,*}

¹ Aerosol and Haze Laboratory, Beijing Advanced Innovation Center for Soft Matter Science and Engineering, Beijing University of Chemical Technology, Beijing 100029, China

² Institute for Atmospheric and Earth System Research, Faculty of Science, University of Helsinki, Helsinki 00014, Finland

³ Laboratory of Atmospheric Chemistry, Paul Scherrer Institute, Villigen, Switzerland.

⁴ Department of Environmental Science, Stockholm University, Stockholm, 11418, Sweden

⁵ Department of Chemistry and Molecular Biology, Atmospheric Science, University of Gothenburg, Gothenburg, SE-412 96, Sweden

⁶ State Key Joint Laboratory of Environmental Simulation and Pollution Control, Beijing Innovation Center for Engineering Science and Advanced Technology, College of Environmental Science and Engineering, Peking University, Beijing, 100871, China

These authors contributed equally to this work.

Correspondence to: kaspar.dallenbach@helsinki.fi and claudia.mohr@aces.su.se

Abstract: Measurements of the molecular composition of organic aerosol (OA) constituents improve our understanding of sources, formation processes, and physicochemical properties of OA. One instrument providing such data at a time resolution of minutes to hours is the Chemical Ionization time-of-flight Mass Spectrometer with Filter Inlet for Gases and AEROSols (FIGAERO-CIMS). The technique collects particles on a filter, which are subsequently desorbed, and the evaporated molecules are ionized and analyzed in the mass spectrometer. However, long-term measurements using this technique and/or field deployments at several sites simultaneously, require substantial human and financial resources. The analysis of filter samples collected outside the instrument (offline) may provide a more cost-efficient alternative and makes this technology available for the large number of particle filter samples collected routinely at many different sites globally. Filter-based offline use of the FIGAERO-CIMS limits this method albeit to particle-phase analyses, likely at reduced time resolution compared to online deployments. Here we present the application and assessment of offline FIGAERO-CIMS, using Teflon and Quartz fiber filter samples that were collected in autumn 2018 in urban Beijing. We demonstrate the feasibility of the offline application with “sandwich” sample preparation for the identified over 900 organic compounds with (1) high signal-to-noise ratios, (2) high repeatability, and (3) linear signal response to the filter loadings. Comparable overall signals were observed between the Quartz fiber and Teflon filters for 12-h and 24-h samples, but with larger signals for semi-volatile compounds for the Quartz fiber filters, likely due to adsorption artifacts. We also compare desorption profile (thermogram) shapes for the two filter materials. Thermograms are used to derive volatility qualitatively based on the desorption temperature at which the maximum signal intensity of a compound is observed (T_{\max}). While we find that T_{\max} can be determined with high repeatability ($\pm 5.7^\circ\text{C}$) from the duplicate tests for one filter type, we observe considerable differences in T_{\max} between the Quartz and Teflon filters, warranting further investigation into the thermal desorption characteristics of different filter types. Overall, this study provides a basis for expanding OA molecular characterization by FIGAERO-CIMS to situations where and when deployment of the instrument itself is not possible.

1. Introduction

42 Molecular information on organic aerosol (OA) composition is important for understanding the role that OA
43 plays in the atmosphere regarding its impacts on air quality, human health, and the climate (Daellenbach et al.,
44 2020; Huang et al., 2014; Cappa et al., 2012; Yao et al., 2018; Riipinen et al., 2012). Such data can be obtained
45 from offline filter collection and analysis in the laboratory using optical (e.g. Fourier transform infrared
46 spectroscopy, FTIR) and magnetic (e.g. Nuclear magnetic resonance spectroscopy, NMR) spectroscopy or, more
47 commonly, high-resolution mass spectrometer methods, which include gas/liquid chromatography coupled to
48 mass spectrometry (GC/LC-MS), ultrahigh-performance liquid chromatography coupled to Orbitrap mass
49 spectrometry and electrospray ionization mass spectrometry (ESI-MS) (Noziere et al., 2015). In contrast, online
50 mass spectrometers provide direct and in-situ information on particles' molecular composition, e.g. the filter inlet
51 for gases and aerosols coupled to a high-resolution time-of-flight chemical ionization mass spectrometer
52 (FIGAERO-HR-ToF-CIMS, Aerodyne Research Inc., US, hereafter FIGAERO-CIMS (Lopez-Hilfiker et al.,
53 2014)) or the extractive electrospray ionization time-of-flight mass spectrometer (EESI-MS) (Lopez-Hilfiker et
54 al., 2019). Since the particle-phase measurement by FIGAERO-CIMS is filter-based, it has the potential to be used
55 for offline analysis. Briefly, in the FIGAERO, particles are collected on a Teflon[®] (hereafter Teflon) filter and
56 analyzed via thermal desorption. When coupled to a high-resolution time-of-flight chemical-ionization mass
57 spectrometer (hereafter CIMS), molecular composition information of inorganic and organic aerosol compounds
58 that evaporate at temperatures up to 200 °C can be achieved. Having the advantage of combining molecular
59 composition and volatility information, the FIGAERO-CIMS has been widely used for measuring OA compounds
60 in many different environments including e.g. forests (Lopez-Hilfiker et al., 2016; Lee et al., 2016; Lee et al., 2018;
61 Mohr et al., 2019), rural and urban areas (Le Breton et al., 2019; Huang et al., 2019b; Cai et al., 2022), indoor air
62 (Farmer et al., 2019), and cooking emissions (Masoud et al., 2022).

63 Both online and offline techniques have their advantages and disadvantages and are associated with artefacts
64 (Turpin and Lim, 2001; Turpin et al., 2000). Both online and offline techniques have their advantages and
65 disadvantages and are associated with artefacts (Turpin and Lim, 2001; Turpin et al., 2000). Offline techniques
66 are an easy alternative to demanding online in-situ approaches requiring large human and financial resources.
67 Moreover, one collected filter can be used for different analysis methods and purposes. However, the offline
68 approaches are susceptible to sample handling and storage artefacts. The condensation and re-evaporation of
69 vapors, and potential reactions on the filter during sampling and storage can result in both positive and negative
70 sampling biases (Turpin et al., 2000; Cheng et al., 2009). Online instruments generally allow for measurements at
71 higher time resolution, which is an advantage when studying rapid atmospheric processes, and no sample storage
72 is needed before analysis. However, the deployment of the FIGAERO-CIMS outside the laboratory requires a
73 well-equipped site that is easily accessible. In addition, long-term maintenance of these complex mass
74 spectrometers needs substantial human and financial resources. Therefore, deployments are often achieved only
75 for short periods (i.e. campaigns lasting from a couple of weeks to months), which limits the application of this
76 technique for monitoring and simultaneous measurements at multiple sites. Furthermore, FIGAERO gas-phase
77 measurements have to be interrupted regularly for particle-phase analysis in online usage, which could be a
78 problem for measurements requiring high time resolution data (e.g. chamber studies). Using the FIGAERO-CIMS
79 for analyzing filters collected elsewhere ("offline application") may therefore provide a valid alternative for long-
80 term monitoring or simultaneous measurements at multiple sites. Whereas the online FIGAERO-CIMS technique
81 typically uses Teflon filters to reduce interferences from the gas phase, Quartz fiber filters are widely used for
82 offline sampling of OA due to their high melting point and insolubility in water and typical organic solvents
83 (Watson and Chow, 2002; Tao et al., 2017; Schauer et al., 2002; Gustafson and Dickhut, 1997). Up to now, only
84 a few studies have used the FIGAERO-CIMS in offline mode with Teflon filters (Siegel et al., 2020; Huang et al.,
85 2019a), and an in-depth characterization of the method is missing. The performance of Quartz fiber filters in
86 FIGAERO-CIMS needs to be assessed and compared to Teflon filters.

87 Here, we describe the application of FIGAERO-CIMS in offline mode for the analysis of particles deposited on
88 Teflon and Quartz fiber filters in urban Beijing during the autumn and winter of 2018. The filter deposition time
89 varies from 30 min to 24 h. We assess the performance of FIGAERO-CIMS for offline characterization of OA as

90 well as inorganic compounds and discuss background determination, reproducibility, and linearity of response for
91 the two filter types. We describe filter handling and offline analysis procedures and show the comparison of signals
92 from different mass loadings collected on both filter types. The utility of the FIGAERO for offline use is
93 demonstrated in this study. The potential to broaden its application for OA component measurements in future
94 research is also discussed. We note, however, that it is not the scope of this paper to discuss aspects of offline
95 FIGAERO-CIMS that also apply to its online deployment, such as e.g. general percentage of recovery from the
96 filter or calibrations.

97 **2. Methods**

98 **2.1 Filter sampling**

99 The sampling site is situated on the west campus of the Beijing University of Chemical Technology (BUCT, 39°
100 56'31" N, 116°17'50" E). BUCT is located near the West Third Ring Road of Beijing, surrounded by residential
101 areas. A more detailed description of the sampling site can be found elsewhere (Cai et al., 2020; Kontkanen et al.,
102 2020; Liu et al., 2020; Yao et al., 2020; Fan et al., 2021; Guo et al., 2021). From November to December 2018,
103 samples of fine particulate matter with an aerodynamic diameter of up to 2.5 μm ($\text{PM}_{2.5}$) were collected by a four-
104 channel sampler (TH-16A, Tianhong Co., China) with a sampling flow rate of 16.7 L min^{-1} , installed on the rooftop
105 of a five-floor building (~20m above ground). Both Teflon (Zefluor® PTFE membrane, 1 μm pore size, 47 mm
106 diameter, Pall Corp., US) and Quartz fiber filters (7202, 47 mm diameter, Pall Corp., US) were collected
107 simultaneously at separate channels. The four parallel channels of the sampler had a shared PM_{10} cyclone inlet and
108 were equipped with 4 independent $\text{PM}_{2.5}$ cyclones and auto flow controllers for each channel. All channels were
109 measuring the same size range of particles. A sizing effect from the interactions between different channels can
110 therefore be neglected. The setup of filter type for each channel was as follows: Channel 1, Teflon (12 h for or 0.5
111 h); Channel 2, Quartz (12 h or 0.5 h); Channel 3, Teflon (24 h or 2.5 h); Channel 4, Quartz filters (24 h or 2.5 h).
112 This is listed in Table 1. The flow rate was regularly calibrated individually for each channel during the sampling
113 process.

114 To investigate the influence of filter mass loadings and collection time on the signal response, the following filter
115 samples were taken: (1) 5 pairs of samples (Teflon/Quartz fiber filters, Channels 1 and 2) with 30 min deposition
116 time on Dec 15, 2018 between 14:00 to 16:30 (Table 1). At the same time, an additional pair of Teflon/Quartz
117 samples were deposited for 2.5 hours using the other two separate channels of the sampler (Channels 3 and 4). (2)
118 12-h samples of Quartz/Teflon filters (Channels 1 and 2) from Oct 26 to Oct 30 and Nov 3 to Nov 24 (here only
119 the Quartz filters from Nov 3 to Nov 16 were analyzed (in total 27 pairs of samples), shown in Table 1). (3) 24-h
120 Quartz/Teflon samples (Channels 3 and 4) from Oct 26 to Oct 30 and Nov 3 to Nov 25 (here only one pair of
121 Teflon/Quartz filters was analyzed, shown in Table 1). During the last sampling period, high $\text{PM}_{2.5}$ and relative
122 humidity (RH) conditions prevailed (Nov 3: 181 $\mu\text{g m}^{-3}$, 60%, and Nov 13: 227 $\mu\text{g m}^{-3}$, 75%), and the channel of
123 the 24-h sampling Teflon filter got clogged. Thus, only one pair of 24-h Teflon/Quartz samples from this period
124 was analyzed (Table 1).

125 Detailed information on the sampling protocol is listed in Table 1. Three pairs (Teflon/Quartz) of field blank
126 samples were also collected during the sampling period. Before sampling, Teflon filters were baked for 2 hours at
127 200 °C, which is much longer than the typical desorption time for FIGAERO-CIMS online usage (Ylisirmö et al.,
128 2021), and Quartz filters for 4.5 hours at 550 °C (Liu et al., 2016) in order to minimize contamination. After
129 sampling, samples were put in filter holders wrapped in pre-baked aluminum foils, individually sealed in a sealed
130 bag and stored in a freezer at -20 °C for 7 months until being analyzed in the laboratory.

131 To calculate the OA mass loadings of the samples, an online Time-of-Flight-Aerosol Chemical Speciation
132 Monitor (Aerodyne Research Inc., US, hereafter ToF-ACSM) equipped with a $\text{PM}_{2.5}$ lens and standard vaporizer
133 was operated during the sampling period at the same site. Details of the ToF-ACSM settings can be found in Cai

134 et al. (2022). The OA loading on each filter (OA_{filter}) was determined relying on the OA concentrations from the
 135 co-located TOF-ACSM (OA_{ACSM}), the offline filter sampling flow rate (16.7 L min^{-1}), the sampling time, the
 136 surface of the entire offline filter sample (A_{filter}), and the analyzed offline filter sample (A_{punch}) (Equation 1):

$$137 \quad OA_{\text{filter}} = \frac{A_{\text{punch}}}{A_{\text{filter}}} \times OA_{\text{ACSM}} \times \text{Sampling flow rate} \times \text{Sampling time} \quad (1)$$

138 Table 1: Testing objectives, filter deposition dates and times, flows, filter material (T = Teflon, Q = Quartz fiber),
 139 filter mass loadings of OA, number of samples, and number of sample repeats (filter punches) for the same filter.

Testing objective	Sampling date	Sampling time	Filter material	OA loading [μg] per punch (punch diameter, area)	Number of samples/repeats
(1) Baseline subtraction tests, (2) reproducibility tests, (3) filter type comparison	Dec 15 14:00 – 16:30 (30 min-interval)	30 min	T & Q	1.7×10^{-2} – 2.0×10^{-2} (2 mm, 0.031 cm ²)	1/1
	Dec 15 14:00 – 16:30	2.5 h	T & Q	9.1×10^{-2} (2 mm, 0.031 cm ²)	1/3 for repeats
(1) Reheating tests, (2) filter type comparison	Nov 8 21:30– Nov 9 9:00	12 h	T & Q	6.5×10^{-1} (2 mm, 0.031 cm ²)	1/1
Reheating tests	Nov 12 21:30– Nov 13 9:00	12 h	Q	0.75 (2 mm, 0.031 cm ²)	1/1
Reheating tests	Nov 13 21:30– Nov 14 9:00	12 h	Q	1.2 (2 mm, 0.031 cm ²)	1/1
(1) Filter type comparison, (2) different ramping protocols for 2 mm punch, (3) linearity response for signals from different filter punch areas	Nov 24 9:30– 9:00 25	24 h	T & Q	1.2 (2 mm, 0.031 cm ²)	1/3 for repeats and 1/3 for different ramping protocols
				2.7 (3 mm, 0.071 cm ²)	1/1
				4.8 (4 mm, 0.13 cm ²)	1/1

				15 (7 mm, 0.38 cm ²)	1/1
Comparison of 12-h signals to ToF-ACSM	Nov 3 to Nov 16	12 h	Q	5.0×10 ⁻² – 1.2 (2 mm, 0.031 cm ²)	27/1

140

141

142 2.2 Offline application of FIGAERO-CIMS

143 2.2.1 Measurement approach

144 2.2.1.1 FIGAERO-CIMS setup

145 The molecular composition of OA collected on the filter samples was characterized with FIGAERO-CIMS using
 146 iodide (I⁻) as the reagent ion. In typical online FIGAERO-CIMS operation, particles are collected on a filter
 147 (Zefluor[®] Teflon filters) with a sampling time of a few minutes to hours and then thermally desorbed by a flow of
 148 temperature-controlled ultra-pure nitrogen (99.999 %) immediately following deposition. The thermally desorbed
 149 compounds are charged by clustering with I⁻, which is typically generated through the exposure of methyl iodide
 150 to an X-ray or radioactive source for FIGAERO-CIMS (Po²¹⁰ in our study). In this study, we used the FIGAERO-
 151 CIMS in the laboratory to analyze filter samples collected earlier in the field. These samples were placed manually
 152 one by one in the dedicated filter holder of the FIGAERO-CIMS and the desorption procedure was started (see
 153 2.2.1.3).

154 2.2.1.2 Sample preparation and test design

155 Since the total particle mass collected on one filter was generally too large to be analyzed at once in its entirety
 156 by FIGAERO-CIMS (due to the risk of titration of the reagent ion), we only analyzed small circular punches of
 157 the collected filters. The default punching area was 3.1×10⁻² cm² (punch diameter $d=2$ mm). In addition, to test the
 158 linearity of response to sample mass loadings, punch areas for the same filter were varied between 3.1×10⁻² cm²
 159 ($d=2$ mm) and 0.38 cm² ($d=7$ mm), resulting in variation in mass loadings by a factor of 10 (shown in Table 1).
 160 Since the filter punches were too small for the filter holder of the FIGAERO, we put them between two pre-baked
 161 originally sized ($d=25$ mm) Zefluor[®] Teflon filters (“sandwich technique”, Fig. 1a). Field blanks were prepared
 162 analogously.

163 The OA mass loadings of the filter punches were estimated with the co-located ToF-ACSM in this study (details
 164 shown in Table 1). To test the performance of the method, we did the following tests (Fig. 1, Table 1): (1) reheating
 165 a few filters to determine backgrounds (see section 2.2.4), (2) assess different background subtraction methods,
 166 (3) reproducibility of signals from the same filter (section 3.4), (4) the linearity of signal response from different
 167 punching areas from the same filter (section 3.4), (5) comparing signals from different ramping protocols (section
 168 2.2.1.3), (6) comparison between and offline FIGAERO-CIMS and online ToF-ACSM (section 3.5), (7) signals
 169 from different filter types (section 3.6), and (8) thermograms from different types of filters (section 3.7).

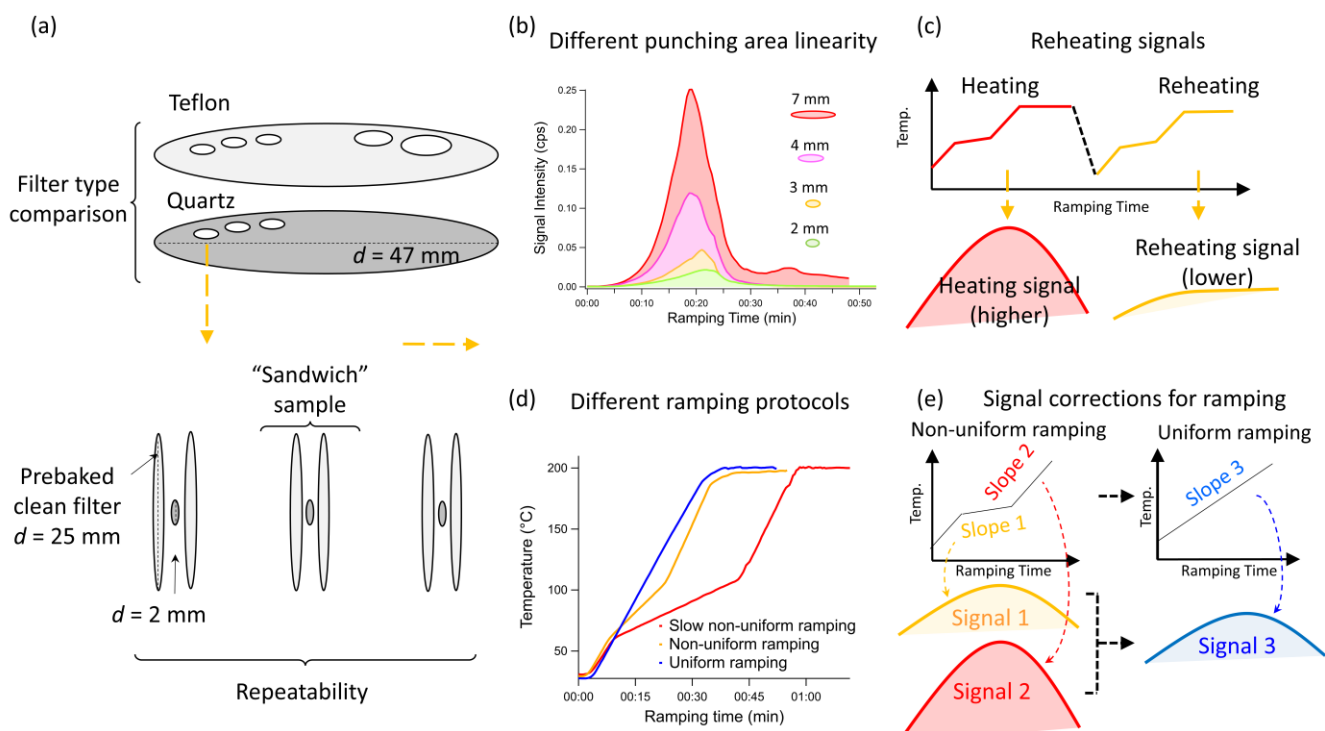
170 2.2.1.3 Temperature ramping protocols

171 Reagent ion depletion is undesired as it can create non-linearities in the instrument response (Koss et al., 2018;
 172 Zheng et al., 2021). To avoid reagent ion depletion in FIGAERO-CIMS, the concentration of sample ions entering

173 the instrument is controlled, typically by modifying the particle mass loading on the filter and/or the heating rate.
174 While the particle mass loading can be varied easily when operating the FIGAERO-CIMS online through
175 adjustment of sampling time and flow, in offline mode with pre-collected samples this can only be modified by
176 the fraction of filter surface analyzed. For our Beijing filter samples, even when using the smallest punch sizes
177 ($3.1 \times 10^{-2} \text{ cm}^2$), mass loadings of especially nitric acid (HNO_3) were still high enough to lead to titration of the
178 reagent ion. We note that this can also be an issue for online measurements in presence of high nitrate
179 concentrations, e.g. in highly polluted areas. In order to reduce reagent ion depletion between 60 °C to 105 °C
180 desorption temperature, where HNO_3 exhibits a maximum signal, we used a heating protocol with a non-uniform
181 temperature ramping procedure. Instead of ramping from room temperature to 200 °C with a constant heating rate,
182 we divided the temperature ramp into several periods: (1) from room temperature ($\sim 25 \text{ °C}$) to 60 °C in 8 min
183 (4.4 °C min^{-1}), (2) from 60 °C to 105 °C in 15 min (3 °C min^{-1}), (3) from 105 °C to 200 °C in 12 min (7.9 °C min^{-1}).
184 The ramp period was followed by a 20-minute soaking period (200 °C) to allow signals to go to background
185 levels. We called this temperature ramping protocol non-uniform temperature ramping and used it as the default
186 desorption procedure in this study. The maximum reagent ion depletion achieved in this way was $\sim 35\%$ for the
187 samples with the highest mass loadings on a 2 mm punch, which was mostly used in this study. We also tested
188 two alternative heating protocols:

- 189 1) Slow non-uniform temperature ramping: Same as the non-uniform ramping protocol, but with (2)
190 slowed down to 1.5 °C min^{-1} . The total heating time for this protocol was 70 minutes, and the
191 maximum reagent ion depletion was $\sim 20\%$.
- 192 2) Uniform temperature ramping: The temperature was increased from room temperature to 200 °C
193 in 31.5 min (5.7 °C min^{-1}). Including the 20 min soak, the total heating was 51.5 minutes, and the
194 maximum reagent ion depletion was around 50%. In order to limit reagent ion depletion, the
195 heating rate was 1.8–3.5 times slower than typical rates used for online FIGAERO-CIMS
196 applications ($10\text{--}20 \text{ °C min}^{-1}$ (Thornton et al., 2020)).

197 The 3 temperature ramping protocols are displayed in Fig. 1d. As different heating rates lead to different
198 thermogram shapes and T_{max} for individual compounds, we developed a correction method in an effort to be able
199 to compare desorption-derived volatility for the different ramping protocols. This will be further discussed in
200 section 3.3.



202

203 **Figure 1.** Schematic of the tests conducted in this study, (a) sample preparation using punching areas of different sizes of the
 204 Teflon and Quartz fiber filters and squeezing them between two original-sized filters for analysis, (b) signal intensities of
 205 different punching areas from the same sample with the same analytical procedure, (c) reheating tests by conducting two
 206 consecutive heating cycles, (d) different temperature procedures, and (e) signal intensity correction from non-uniform
 207 ramping to uniform ramping.

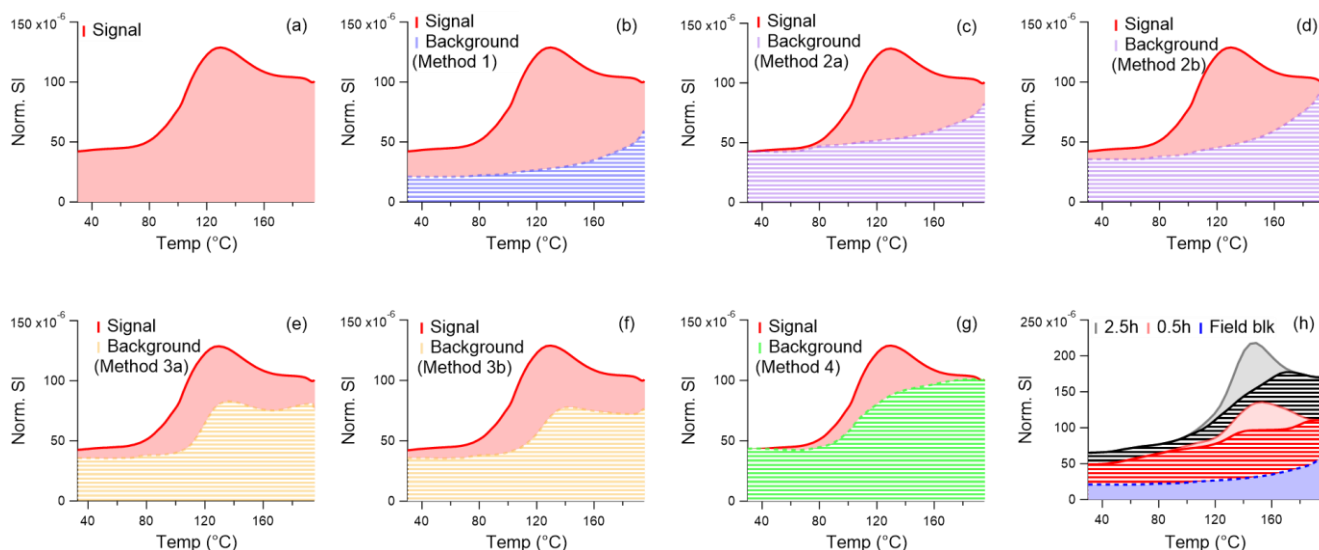
208 2.2.2 Data analysis

209 In this study, FIGAERO-CIMS data were analyzed with the Tofware package (v.3.1.0, Tofwerk, Switzerland,
 210 and Aerodyne, US) within the Igor Pro software (v.7.08, Wavemetrics, US). Mass accuracies of low- to high-mass
 211 species (~ 130 to 500 Da) were within ± 10 ppm for all the samples. A total of $\sim 1,200$ peaks were found in the range
 212 of 46 and 500 Da, of which 916 were identified as organic species. Detailed information about the identified
 213 chemical compounds can be found in Cai et al. (2022). The total signal of a compound per filter sample, defined
 214 as the integrated signals (I_s), calculated by first normalizing by the signals of the primary ions (I^-) and then
 215 integrating the entire thermogram (ramping and soaking, normalized by the signals of I^-). Signals of the first 1.5
 216 min of ramping and the last 1.5 min of soaking periods were excluded in order to remove potential interference
 217 from switching to and from the heating status. In this study, we use the term CHOX to represent all organic
 218 compounds identified by FIGAERO-CIMS, $C_{x \geq 1}H_{y \geq 1}O_{z \geq 1}X_{0-n}$, detected as clustered with I^- , with X being different
 219 atoms including N, S, Cl, or a combination of them.

220 2.2.3 Background subtraction

221 The background in offline FIGAERO-CIMS is a combination of instrument background and field blank. The
 222 field blanks provide information on sampling and handling artefacts, while the instrument background is mainly
 223 from (1) the desorption of semi-volatile or low-volatile compounds adsorbed on instrument surfaces (such as the
 224 ion-molecular reaction region (IMR)), and (2) impurity of the reagent ion precursors and carrier gases. Thus,
 225 instrument background signal can vary for different samples and depending on instrument status. For FIGAERO-
 226 CIMS online deployments, frequent blank measurements and calibrations are recommended (Bannan et al., 2018;

227 Thornton et al., 2020). The common method for online FIGAERO-CIMS of placing an additional filter upstream
 228 of the FIGAERO filter is impossible for offline pre-sampled filters. Given 1) the large variation of the filter sample
 229 loadings ($\sim 1 \times 10^{-2} \mu\text{g} - 1.2 \mu\text{g}$), which influences the number of compounds that can potentially adsorb to
 230 instrument surfaces, 2) the general scarcity of field blanks in offline mode compared to background filter samples
 231 in online FIGAERO-CIMS, and 3) that the instrument background can be influenced by instrument history very
 232 different from the offline sample due to the temporal separation of sample and analysis, choosing an appropriate
 233 instrumental and field blank determination method is crucial and challenging for offline FIGAERO-CIMS analysis.
 234 Here we describe and discuss performance of 6 different background subtraction methods (schematically shown
 235 in Fig. 2):



236

237 **Figure 2.** Schematic of a compound's signal and background thermograms for different background determination methods.
 238 The x-axis is the temperature during ramping, and the y-axis is the signal intensity normalized by the primary ion (I^+). (a) total
 239 sample signal of a model compound without blank subtraction, (b) Method 1: field blank only, (c) Method 2a: scaling field
 240 blank to the start of ramping, (d) Method 2b: scaling field blank to the end of soaking, (e) Method 3a: reheating of a subset
 241 of filters, and using the average signal ratio from reheated and heated filters as background signal for all filters (individual
 242 compound-based), (f) Method 3b: reheating of a subset of filters, and using an exponential fit to the entire mass range of the
 243 average signal ratio from reheated and heated filters as background signal for all filters, (g) Method 4: thermal baseline using
 244 a spline algorithm, and (h) one 0.5-h and one 2.5-h sample with blank-subtraction. Ideally, the I_s of the 2.5-hour collection
 245 sample ($I_{S_{2.5h}}$) would be close to the sum of the 5 paralleled 0.5-hour collection sample ($I_{S_{0.5h}}$).

246 **Method 1:** Background is the average integrated signal intensity (I_s , the integrated signal of the thermograms
 247 shown in Fig. 2a) of field blanks ($\overline{I_{S_{field\ blk,l}}}$), which are three in our case (Fig. 2b). The integrated background-
 248 subtracted signal for compound i ($I_{S_{blksub,i}}$) is then $I_{S_i} - \overline{I_{S_{field\ blk,l}}}$.

249 **Method 2:** Background is field blank average ($\overline{I_{S_{field\ blk,l}}}$, see Method 1) scaled to the ratio of ambient sample
 250 and field blank signals during a reference period (ref period) – either prior to the start of heating (the first 1.5 to 3
 251 min of the ramping procedure before the temperature starts to increase, Method 2a or at the end of the soaking (the
 252 last 1.5 to 3 min of the soaking period, Method 2b). Method 2 corrects for variation in instrument background that
 253 is not necessarily related to the sample to be analyzed. The integrated background-subtracted signal for compound
 254 i ($I_{S_{blksub,i}}$) is then

255

$$I_{S_{blksub,i}} = \int I_{sample,ij} - \int I_{field\ blk,ij} \times \frac{\int^{ref\ period} I_{S_{i,ambient}}}{\int^{ref\ period} I_{S_{i,field\ blk}}} \quad (2)$$

256 By using Method 2a, it is assumed that the signal measured before heating, but with the filter already in place, is
 257 due to instrument background, which can vary between the measurement of a sample filter and a blank filter (Fig.
 258 2c). However, this method may lead to underestimation of the sample signal for compounds that already evaporate
 259 at room temperature.

260 By using Method 2b, it is assumed that the signal measured at the end of soaking is due to instrument background,
 261 which can vary between the measurement of a sample filter and a blank filter. The variation in instrument
 262 background is taken into account at maximum heating temperature (200 °C) and thus elevated temperature of
 263 surfaces downstream of the filter, and at the end of the soaking period when presumably all material that can
 264 evaporate from the filter has evaporated (shown in Fig. S1).

265 **Method 3:** In this method (Siegel et al., 2021), the instrument background is assessed by heating the same filter
 266 twice, assuming that during the first heating cycle, all detectable material has evaporated, and that what is measured
 267 in a reheating cycle is the instrument background signal. Ideally, reheating would be done for each sample
 268 individually. Since this was not done for our dataset, the instrument background determined based on a few reheats
 269 (3 in our case, the details of the reheating samples are shown in Table 1) had to be extrapolated to all samples
 270 (Method 3a and 3b). It is clearly shown that the signals from the reheating cycle are much lower than those from
 271 the first heating (Fig. S1) without a clear peak in thermograms for both filter types, suggesting sampled compounds
 272 were well desorbed in the original heating cycle. Simple reheating does not consider the field blanks, which need
 273 to be subtracted in addition.

274 For Method 3a we assumed that the ratio of the integrated signal of the second heating cycle (heating C2) and first
 275 heating cycle (heating C1) of the same filter is influenced by volatility and therefore compound-dependent. Here
 276 we used the average ratio from 3 reheating tests done for this dataset (Fig. S2). The distribution of the ratios is
 277 shown in Fig. S3. The $IS_{blksub,i}$ was then calculated following Eq. 2, where the instrument background is the fraction
 278 of the sample signal established from the re-heating, and added to the signal from the field blank, which is
 279 calculated in the same way.

$$280 \quad IS_{blksub,i} = \left(IS_{sample,i} - IS_{sample,i} \times IS_{i, \left(\frac{heating\ C2,i}{heating\ C1,i} \right)} \right) \\ 281 \quad - \left(IS_{field\ blk,i} - IS_{field\ blk,i} \times IS_{i, \left(\frac{heating\ C2,i}{heating\ C1,i} \right)} \right) \quad (3)$$

282 For Method 3b, we assumed that the ratio of heating C2 to heating C1 exhibits a signal dependency (relatively
 283 higher background for compounds with lower signal), calculated using an exponential fit to the data from the 3
 284 reheat tests (Fig. S4) using Eq. (4) with the constants A, B, and C. The field blanks are calculated in the same way.
 285 Then the IS_{blksub} can be calculated as in Eq. (3)

$$286 \quad IS_{i, \left(\frac{heating\ C2,i}{heating\ C1,i} \right)} = A + B \times \exp(IS_{sample,i} + C) \quad (4)$$

287 **Method 4:** Thermal baseline subtraction. In this method, we determined for every thermogram of each compound
 288 a background thermogram termed thermal baseline (IS_{thbsl}). The thermal baseline was computed using a spline
 289 algorithm initially developed by Wang et al. (2018) for determining the background concentration of a pollutant
 290 using its concentration time series (by determining the spline of background from varying time intervals).
 291 Thermogram data were pre-averaged to 1.8 mins (corresponding to 4 data points of the original time resolution of
 292 27s) to reduce noise for the thermal baseline computation. Field blanks were handled in the same way (shown in
 293 Fig. S5). Thus, the blank-subtracted signal IS_{blksub} of a compound i is:

$$294 \quad IS_{blksub,i} = IS_{sample,blksub,i} - IS_{field\ blk,blksub,i} \\ 295 \quad = \left(\int IS_{sample,i,j} - IS_{sample,thbsl,i} \right) - \left(\int IS_{field\ blk,i,j} - IS_{field\ blk,thbsl,i} \right) \quad (5) \\ 296$$

297 $I_{s_{sample, thsbl,i}}$ and $I_{s_{field\ blk, thsbl,i}}$ represent the thermal baseline of compound i for samples and field blanks, respectively.

298 2.2.4 Thermograms and T_{max} recovery

299 The amount of compounds coming off the filter at a certain temperature varies as a function of temperature
300 ramping rates, resulting in different thermogram shapes and T_{max} (shown in Fig. 1d). This is especially important
301 in our case for the non-uniform ramping protocols. In an attempt to make the different cases comparable for
302 qualitative volatility studies, we developed a thermogram correction where the blank-subtracted signal as a
303 function of temperature for each compound i is re-distributed to constant temperature intervals (Eq. (6)):

$$304 \quad I_{thermocorrected,i,j} = \int_{T-\Delta T}^T I_{sample,blksub,i,j} dT \quad (6)$$

305 Considering the ~ 2 °C variation in thermogram reproducibility reported from an online FIGAERO-CIMS study
306 (Lopez-Hilfiker et al., 2014), the temperature interval ΔT used in this study is 3°C.

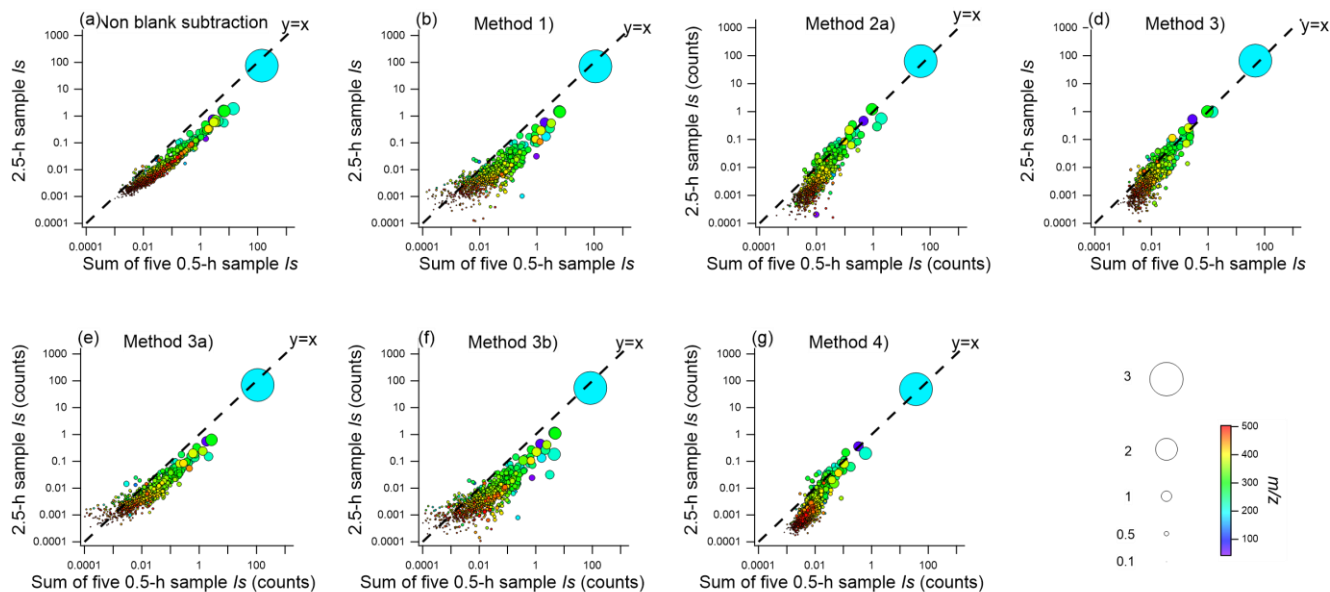
307

308 3. Results

309 3.1 Assessment of the background: Signal comparison between different blank subtraction methods

310 To assess the influence of the 6 background methods on the resulting signal, Quartz fiber filter samples from 5
311 different 0.5-h samples (OA: $\sim 2.0 \times 10^{-2}$ μg for each punch) and a 2.5 h sample collected in parallel (OA: 9.1×10^{-2}
312 μg) were used, and the sum of their background-subtracted integrated signals ($I_{s_{blksub}}$) compared (Fig. 2 h). Without
313 background subtraction, the sum of the signals from the five 0.5-h samples was generally higher than the I_s of the
314 2.5-h sample (shown in Fig. 3a). An exception to this is HNO_3^- , which has the highest signal of all compounds and
315 therefore is the least influenced by background. The higher I_s for the sum of the five 0.5-h samples is likely because
316 of the low signal-to-noise ratio compared to the 2.5-h sample. Subtracting only the field blank (Method 1) therefore
317 yielded the same result (Fig. 3b). Scaling the heating baseline (Method 2a and 2b) led to a better agreement between
318 the sum of the five 0.5-h and the 2.5-h samples (Figs. 3c and d). Compounds with high abundance generally fall
319 on a 1:1 line (slope range 0.5–2) by using these two background subtraction methods. With the thermal baseline
320 subtraction method (Method 4), results were comparable between 2.5-h and five 0.5-h samples. For the approach
321 using filter reheating (Method 3), there was a lesser agreement between the sum of the 0.5-h samples and the 2.5-
322 h sample (Figs. 3e and 3f). We speculate that this could be improved with a reheating cycle for every sample. For
323 future offline FIGAERO-CIMS analyses, we recommend carefully determining the background. Following our
324 assessment of blank determination methods, we suggest regular collections of field blanks and scaling their signal
325 (Methods 2a/b), and if field blanks are not available, computing a thermal baseline (Method 4). If using the
326 reheating approach as in a previous study with FIGAERO-CIMS in offline mode (Siegel et al., 2021), the
327 background should be determined by conducting reheating desorption cycles for each sample and blank
328 individually.

329 In general, as expected, high mass loadings are less sensitive to the various background subtraction methods due
330 to the higher signal-to-noise ratio (for example, 12-h/24-h sampling with OA loading of ~ 1 μg , Fig. S6). Besides
331 filter loadings, baseline levels can also be influenced by the properties of compounds (e.g. stickiness) and
332 instrument geometry. In summary, of all background subtraction methods shown here, Methods 2a, 2b, and 4
333 achieved the best agreement in signal intensities between the sum of 0.5-h and 2.5-h samples (Fig. S7). With these
334 methods, 82% to 93% of high-signal compounds (25% highest signal) fell into a signal ratio of ~ 1 (0–2, Fig. S8).
335 This shows the importance of correctly assessing the instrument background, especially for compounds with low
336 signal.



337

338 **Figure 3.** Comparison of the integrated signals (I_s) for the 2.5-h versus sum of 0.5-h samples (a) without blank subtraction,
 339 with blank subtraction using (b) Method 1, (c) Method 2a, (d) Method 2b, (e) Method 3a, (f) Method 3b, (g) Method 4. The
 340 size of dots is proportional to the 4th root of integrated signal intensities of compounds, and they are color-coded by the ions'
 341 m/z (mass-to-charge ratio).

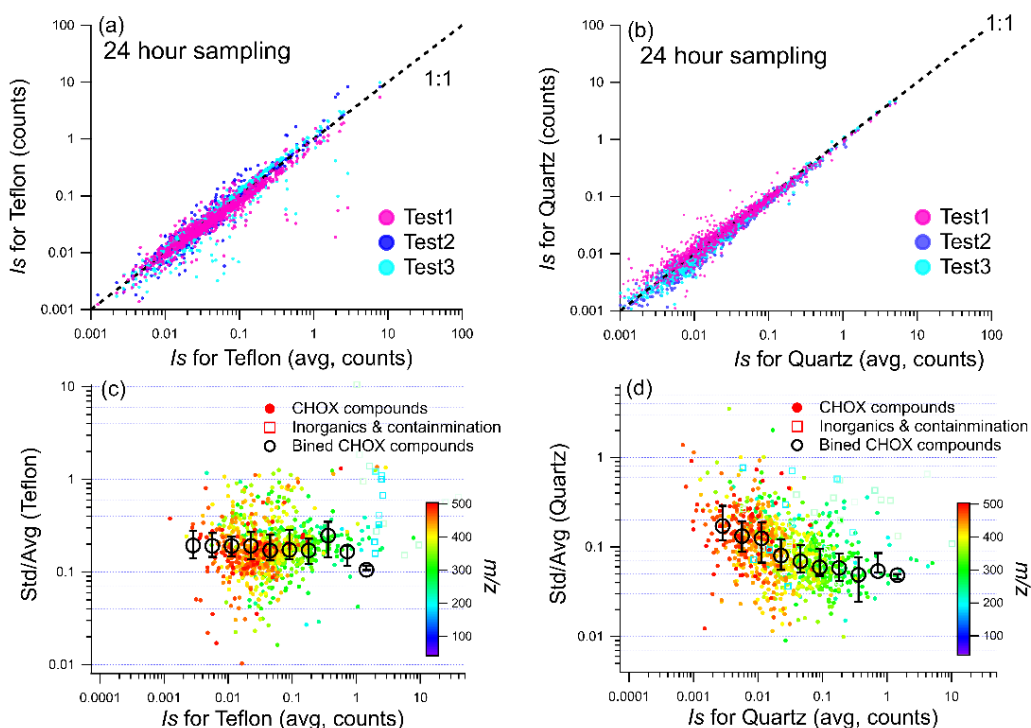
342 In this study, we applied Method 2b in the following discussions due to its better performance for the compounds
 343 with both higher ($I_s > 0.1$ counts) and lower signal ($I_s < 0.01$ counts, Fig. 3d). First, we examined the signal-to-noise
 344 ratios for offline FIGAERO-CIMS, defined as the ratio of the blank-subtracted signal to the standard deviation
 345 (STDs) of the background determined using method 2b per compound. Most of the identified compounds are
 346 above the estimated detection limit (3 times STDs of the backgrounds) for both filter types (87% and 87% of
 347 CHOX peaks for both 24-h Quartz and Teflon filters, OA loadings of $1.2 \mu\text{g}/3.1 \times 10^{-2} \text{cm}^2$ (2 mm punch)). For the
 348 12-h samples (OA loadings of $0.58 \mu\text{g}/3.1 \times 10^{-2} \text{cm}^2$ (2 mm punch)), 84% and 70% of CHOX compounds were
 349 above the detection limit for Quartz and Teflon filters, respectively (Fig. S9). This varies for different filter
 350 loadings and punch areas.

351 3.2 Reproducibility of signal

352 We performed reproducibility tests using three 2-mm punches from the same 24-h and 2.5-h samples of both
 353 Teflon and Quartz filters and checked the signal response with the non-uniform temperature ramping procedure.
 354 The comparisons of the blank-subtracted CHOX I_s for the 24-h and 2.5-h sample punches for both filter types are
 355 displayed in Fig. 4 and Fig. S10, respectively.

356 In Figs. 4a and 4b, we plotted the compounds' signal from one punch versus their average signal from all 3
 357 punches for the Teflon and Quartz filters, respectively. We observe a high correlation between the individual and
 358 average signals (Spearman correlation coefficients R_{sp} are 0.95–0.96 and 0.97–0.99 for Teflon and Quartz filters,
 359 respectively). For each CHOX compound, we also computed the relative error (standard deviation/average signals
 360 ($\text{Std}(I_s)/\text{Avg}(I_s)$) for the three punches) versus the average signal (Figs. 4c, 4d). The relative error for a CHOX
 361 compound was 9% for Quartz and 18% for Teflon (median relative errors) for 24-h samples (Figs. 4c, 4d). The
 362 relative error decreased with higher signal intensities (Figs. 4c, 4d), especially for the Quartz filters, suggesting
 363 that abundant compounds are measured more precisely than less abundant compounds. This trend is less apparent
 364 for Teflon filters, which is likely caused by less reproducibility for high I_s compounds. Possible explanations could
 365 be uneven distribution of particulate mass on the filter or larger uncertainties in the punching process for Teflon
 366 filters due to the extension of the material. 86% and 94% of all CHOX compounds for Teflon and Quartz filters,
 367 respectively, had >3 times higher signals than the variability from the duplicate tests (Fig. S9). For the 2.5-h filter

368 samples (Fig. S10), the relative error is higher compared to the 24-h samples (25% for Quartz, and 31% for Teflon).
 369 This is likely due to the lower OA loadings ($9.1 \times 10^{-2} \mu\text{g/punch}$) of the 2.5-h sample compared to the 24-h sample
 370 ($1.2 \mu\text{g/punch}$), which leads to higher uncertainties for blank subtraction and peak fitting. Still, the analytical
 371 reproducibility is acceptable, even for samples with OA loadings as low as $\sim 0.1 \mu\text{g}$. The relative error between
 372 repeats reported here is slightly larger ($\sim 9\%$ and 18% for $\sim 1 \mu\text{g}$ OA/punch for Quartz and Teflon filters, and 25%
 373 for Quartz, 31% for Teflon for $\sim 0.1 \mu\text{g}$ OA/punch) compared to the variability in signal for online FIGAERO-
 374 CIMS ($5\text{--}10\%$ for $1 \mu\text{g}$ OA, (Lopez-Hilfiker et al., 2014)).



375

376 **Figure 4.** Comparison of the integrated signals from duplicate tests of the same 24-h sample for (a) Teflon and (b) Quartz
 377 fiber filters. The relative error (I_s ratio of standard deviation/average) value of the 3 duplicate tests as a function of I_s for (d)
 378 Teflon and (d) Quartz filters. In (c) and (d), CHOX compounds are shown as dots, inorganics as well as contaminants as
 379 squares colored by the m/z . The black cycles in (c) and (d) represent median values of signal intensity bins (with log I_s intervals
 380 of 0.3 for the I_s range of 0 to 2) and error bars represent the 25th and 75th percentile of binned values of $\text{Std}(I_s)/\text{Avg}(I_s)$ for
 381 CHOX.

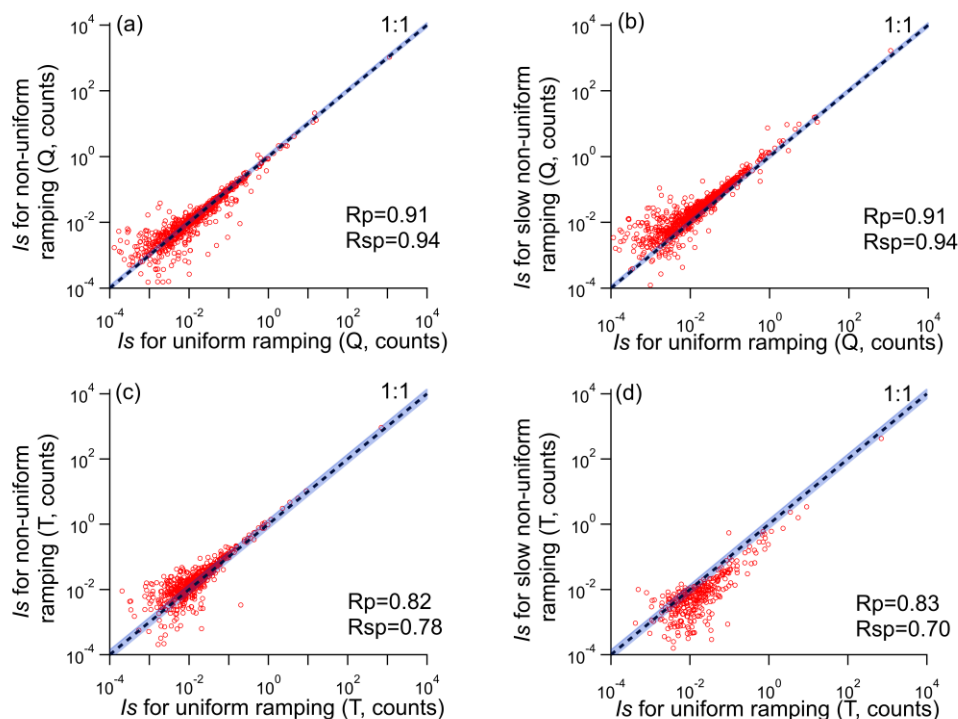
382 3.3 Comparison of signal for different temperature ramping protocols

383 Here we compare the signal from different ramping protocols for the punches from the same 24-h Quartz and
 384 Teflon filters (Table 1). Since as suggested in the section 2.2.2, the I_s were calculated by the integration of the
 385 normalized signals (normalized to the primary ion (I^-)), which to some extent compensates for reagent ion
 386 depletion. The signal of the field blanks is largely dominated by instrument background (i.e. there is no distinct
 387 peak in the thermogram (Fig. S1e) thus the I_s of the field blanks is highly influenced by integration time. Since
 388 the field blanks were only analyzed with non-uniform ramping, the I_s for slow non-uniform and uniform ramping
 389 protocols were assumed as the I_s of non-uniform scaled by their integration time ratios.

390 The comparison of the background-subtracted I_s of all identified compounds from different ramping protocols
 391 for a pair of 24-h Quartz and Teflon filters each is shown in Fig. 5. Since the integrated signals of the compounds
 392 within a mass spectrum are log-normally distributed (shown in Fig. S11a and S11b), a linear fit would be strongly
 393 biased by high-signal compounds such as HNO_3I^- or $\text{C}_6\text{H}_{10}\text{O}_5\text{I}^-$. Thus, we calculated the correlation coefficients of

394 the log-transformed signal intensities in the comparison. The Pearson correlation coefficients (R_p) and Spearman
 395 correlation coefficients (R_{sp}) are as follows: for Quartz filters $R_p = 0.91$, $R_{sp} = 0.94$ for non-uniform vs uniform,
 396 and $R_p = 0.91$, $R_{sp} = 0.94$ for slow non-uniform vs uniform, and for Teflon filters $R_p = 0.82$, $R_{sp} = 0.78$ for non-
 397 uniform vs uniform, and $R_p = 0.83$, $R_{sp} = 0.70$ for slow non-uniform vs uniform protocols.

398 These numbers suggest that the Quartz samples were less affected by different temperature ramping protocols
 399 than the Teflon samples. We also note that Teflon samples exhibited lower reproducibility than Quartz samples
 400 (see section 3.2). The lowest R_p and R_{sp} were observed for the comparison between the slow non-uniform ramping
 401 and the uniform ramping procedure for Teflon filters (Fig. 5d). Possible explanations could be the higher
 402 background and thus lower signal-to-noise ratios for Teflon filters in the low ramping rate region ($1.3\text{ }^\circ\text{C min}^{-1}$ for
 403 the range of $60\text{ }^\circ\text{C}$ to $105\text{ }^\circ\text{C}$) of the slow non-uniform ramping protocol. Thus, care needs to be taken when using
 404 very slow heating rates and backgrounds need to be carefully assessed, especially for Teflon filters.



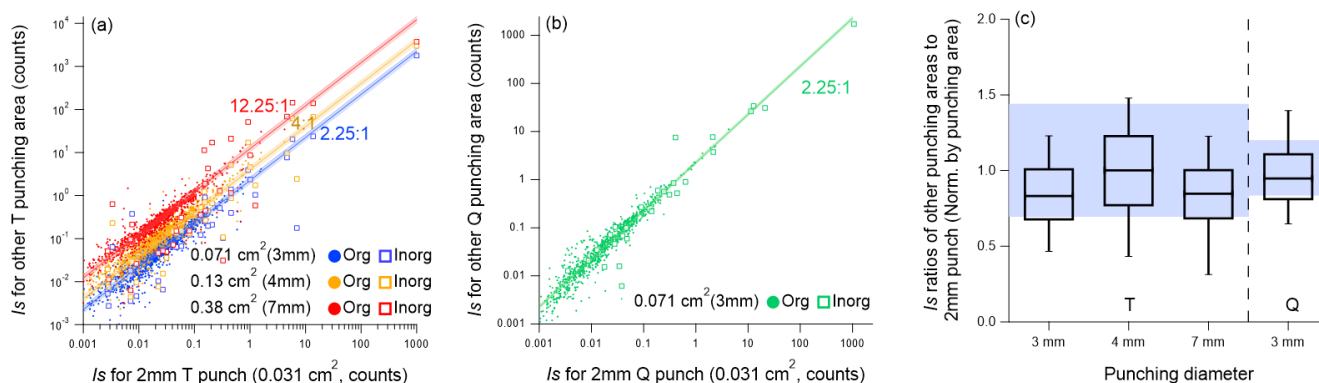
405

406 **Figure 5.** Comparison of I_s from the different temperature ramping protocols of the 24-h Quartz (Q) and Teflon (T) filter
 407 samples, (a) non-uniform and uniform ramping (Quartz sample), (b) slow non-uniform and uniform ramping (Quartz sample),
 408 (c) non-uniform and uniform ramping (Teflon sample), (d) slow non-uniform and uniform ramping (Teflon sample). The blue
 409 shaded areas represent the relative error of signal assessed in the reproducibility tests of the 24-h samples (18% for Teflon
 410 and 9% for Quartz filters). The upper and lower limits for the reproducibility-based variation are calculated as $(1+18\%)/(1-$
 411 $18\%)$ and $(1-18\%)/(1+18\%)$, respectively. The upper and lower limits for the I_s distribution of Quartz caused by
 412 reproducibility are calculated as $(1+9\%)/(1-9\%)$ and $(1-9\%)/(1+9\%)$, respectively.

413 For further analyses, we use the results from the non-uniform temperature ramping protocol, which represents a
 414 good balance between the influence of background due to low signal-to-noise ratios, and I^- depletion. The good
 415 agreement between offline FIGAERO-CIMS and ToF-ACSM discussed in Section 3.5 further implies that such a
 416 ramping protocol is suitable for the OA loadings observed in our study.

3.4 Linearity of signal response

To assess the linearity of signal response to the amount of sample collected on the filter, we used punches with varying areas from one single filter. We used punch diameters of 2, 3, 4, and 7 mm for a Teflon filter and 2 mm and 3 mm for a Quartz filter. The analytical protocol was kept constant between the individual sample punches (non-uniform ramping protocol and method 2b for background subtraction). The mass loadings of the analyzed filter punches ranged from 1.2 to 15 μg OA (2.2 to 27 μg $\text{PM}_{2.5}$) for the Teflon filter and from 1.2 to 2.7 μg OA (2.2 to 5.0 μg $\text{PM}_{2.5}$) for the Quartz filter (Table 1). The blank-subtracted I_s from the different punching areas for the Quartz and Teflon filters is shown in Fig. 6. Overall, the offline FIGAERO-CIMS approach responds linearly to changes in filter mass loadings. The integrated signal ratios of CHOX are consistent with their respective area ratios (Figs. 6a, 6b), within uncertainty. In Fig. 6c we also plot the signal ratios of the 2 mm punch to the other punches, normalized by punching area (where 1 signifies perfect linearity). These ratios are generally in the range of possible variability caused by the relative error from the reproducibility tests.



430

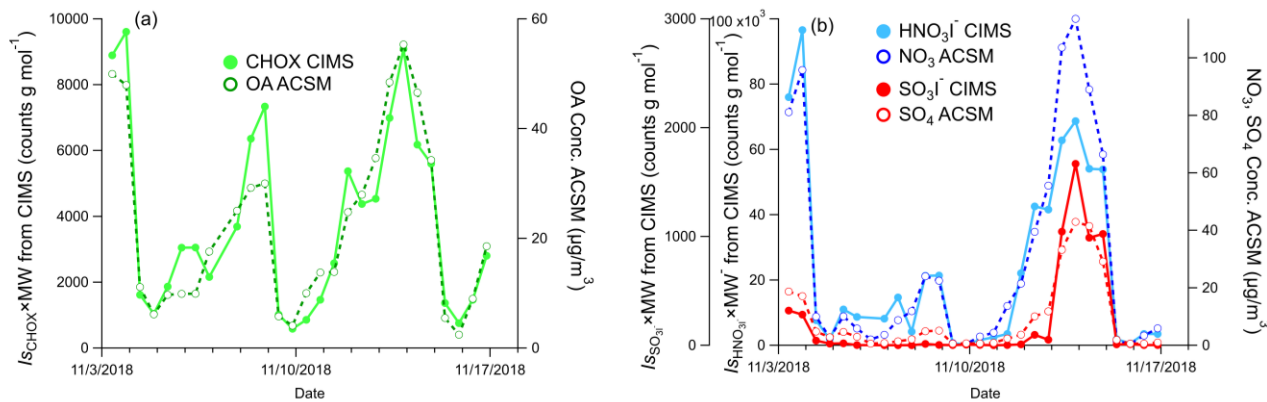
Figure 6. Comparison of the I_s between signals from punches (a) with 3 mm, 4 mm, 7 mm, and 2 mm in diameter for the same Teflon filter, and (b) with 3mm and 2 mm in diameter for the same Quartz filter. The lines in (a) and (b) represent the punching area ratios. The shaded areas in (a) and (b) represent the area ratio plus/minus the relative errors (9% for Quartz, and 18% for Teflon) from the reproducibility tests. (c) Distribution of I_s ratios normalized by the punching area ratios (3 mm, 4 mm, and 7 mm to 2 mm diameter punches for Teflon, 3 mm to 2 mm diameter punches for Quartz). Within each box, the median (middle horizontal line), 25th and 75th percentiles (lower and upper ends of the box), and 10th and 90th percentiles (lower and upper whiskers) are shown. The shaded area in (c) represents the possible distribution of the I_s ratios due to the relative error established from the 24-h sample reproducibility tests (18% for Teflon and 9% for Quartz filters). The upper and lower limits for the Teflon I_s ratio distribution are calculated as $(1+18\%)/(1-18\%)$ and $(1-18\%)/(1+18\%)$, respectively. The upper and lower limits for the Quartz I_s ratio distribution are calculated as $(1+9\%)/(1-9\%)$ and $(1-9\%)/(1+9\%)$, respectively.

For compounds with very high signals, the response I_s ratio can deviate from the punch area ratio, not least also due to the varying degree of reagent ion depletion. The highest I⁻ depletions were ~35%, ~60%, ~68%, and ~70% for 2mm, 3mm, 4mm, and 7mm punches, respectively. For e.g. the highest inorganic (HNO_3I^-) and organic ($\text{C}_6\text{H}_{10}\text{O}_5\text{I}^-$) ions, the I_s from a 7mm punch is only 30% and 67%, respectively, of what would be expected based on punching area ratios (7mm to 2mm). For smaller punches (4 mm/3 mm), 75%/80% and 105%/107% of the expected HNO_3I^- and $\text{C}_6\text{H}_{10}\text{O}_5\text{I}^-$ signals, respectively, are detected. This indicates that for reduced amounts of desorbing material provided by smaller filter fractions, the amount of reagent ion is sufficient during the whole ramping process (lowest $\text{I}^-/\text{C}_6\text{H}_{10}\text{O}_5\text{I}^-$ signal ratio: $\sim 10^3$). In other words, if titration of reagent ion can be avoided as much as possible (e.g. $\text{I}^-/\text{target ion}$ signal ratio: $\sim 10^3$) the I_s responds linearly to concentration changes. In this study, titration is non-apparent for OA loadings of $<5 \mu\text{g}$ and I^- signals of ~ 1 million. Therefore, it is recommended to calculate OA loadings of the samples prior analysis to determine the punching sizes in offline FIGAERO-CIMS analysis.

454 **3.5 Comparison between offline FIGAERO-CIMS and *in-situ* ToF-ACSM**

455 In the following, we compare the time series of the signals from offline FIGAERO-CIMS from Quartz filters and
 456 the corresponding chemical components from online ToF-ACSM measurement. The comparison between the total
 457 signal of all identified CHOX compounds and OA concentrations from the ToF-ACSM is displayed in Fig. 7a.
 458 Here, the FIGAERO-CIMS signals of five polyols ($C_8H_{18}O_5I^-$, $C_{10}H_{22}O_6I^-$, $C_{12}H_{26}O_7I^-$, $C_{14}H_{30}O_8I^-$, $C_{16}H_{34}O_9I^-$)
 459 were excluded, which were contaminants from the lab due to their inexplicably high I_s in 3 of the 27 12-h samples
 460 and the usage of diethylene glycol (DEG) in the lab. To compare with the $PM_{2.5}$ component concentrations from
 461 the ToF-ACSM, for each 12-h filter, we compute the sum of integrated signals (I_s , signal integration over the
 462 entire thermogram, counts) multiplied by their molecular weight (MW, $g\ mol^{-1}$) of all compounds from FIGAERO-
 463 CIMS for comparison to the corresponding $PM_{2.5}$ component concentrations from the ToF-ACSM. Even though
 464 I^- is selective towards oxygenated organic compounds, the total MW-weighted CHOX signal measured by offline
 465 FIGAERO-CIMS in this study highly correlates with OA measured by the ToF-ACSM ($R_p = 0.94$), which is
 466 known to be dominated by secondary organic aerosols (SOA) (Cai et al., 2020; Kulmala et al., 2021; Jia et al.,
 467 2008).

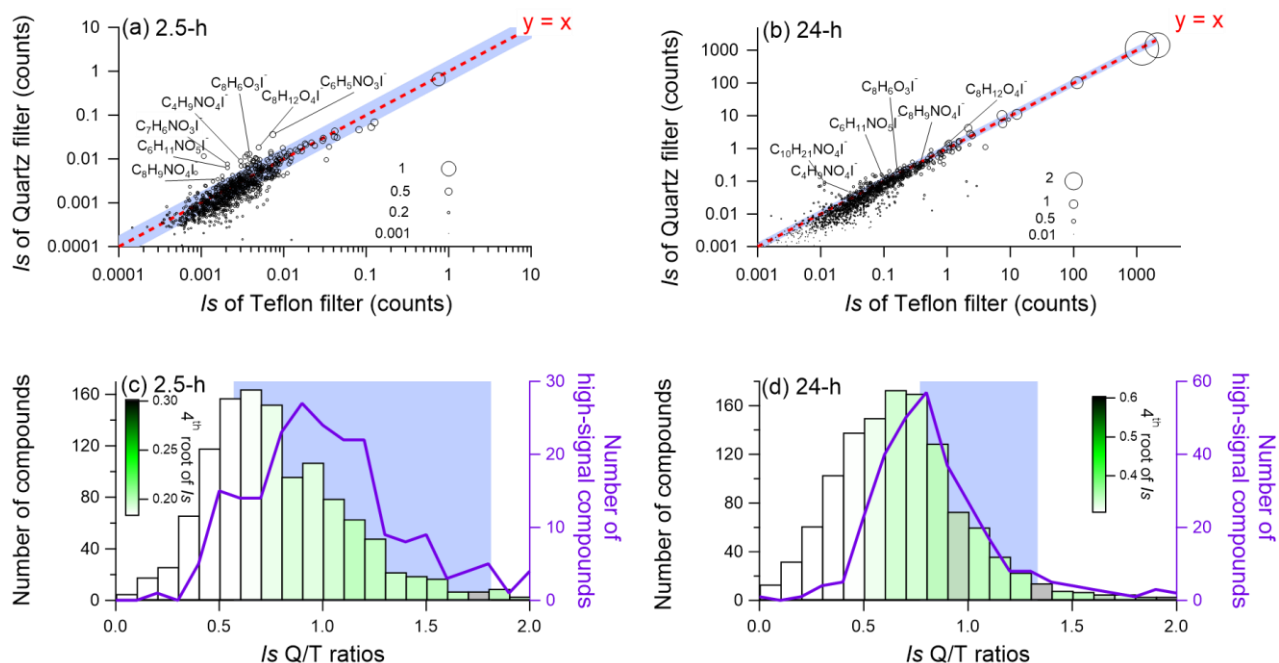
468 The time series of the 12h- I_s for HNO_3I^- and SO_3I^- measured by offline FIGAERO-CIMS correlate well with the
 469 NO_3 and SO_4 concentrations from ToF-ACSM ($R_p = 0.94$ and 0.95 , Fig. 7b). The signal of HNO_3I^- in the particle
 470 phase measured by FIGAERO-CIMS is as an indicator of particulate nitrate and organonitrate (Lee et al., 2016),
 471 and the signal of SO_3I^- is related to inorganic sulfate and sulfur-containing organics (Ye et al., 2021; Cao et al.,
 472 2019). Following the same method, after calibrations, the quantified CHOX mass concentrations of offline
 473 FIGAERO-CIMS were found to be highly correlated with OA and SOA from ToF-ACSM in another dataset at
 474 the Peking University campus (PKU) in Beijing, indicating offline FIGAERO-CIMS analysis can be quantitative
 475 with proper calibrations (shown in Fig. S12 (Zheng et al., 2021)). Like other offline sampling methods, the offline
 476 FIGAERO-CIMS method may be affected by artefacts from sampling and storage of the filters. Both positive
 477 (absorption of gaseous OA), and negative artefacts (volatilization of collected OA), may occur during the sampling
 478 and storage, even if filters were stored frozen (Cheng et al., 2009). However, the signals from FIGAERO-CIMS
 479 correlate generally well with major components measured by TOF-ACSM, suggesting that those artefacts can be
 480 considered minor in our study, at least in terms of bulk PM constituents (Figure 7).
 481



482
 483 **Figure 7.** Comparison of the time series of the integrated signals of inorganic and organic compounds from 12-h samples (2
 484 mm punches) analyzed by offline FIGAERO-CIMS, and chemical components measured in-situ by ToF-ACSM, (a) total
 485 CHOX from FIGAERO-CIMS and OA from ToF-ACSM, (b) HNO_3I^- from FIGAERO-CIMS and NO_3 from ToF-ACSM,
 486 (c) SO_3I^- from FIGAERO-CIMS and SO_4 from ToF-ACSM. To compare with the $PM_{2.5}$ component concentrations from the
 487 ToF-ACSM, the I_s of each compound from FIGAERO-CIMS was multiplied by their molecular weight (MW) in (a) and (b).
 488 Note that FIGAERO-CIMS and ToF-ACSM data are on different axes

3.6 Comparison of Quartz and Teflon filters

489 In the following, we compare the I_s from simultaneously collected Quartz and Teflon filter samples (collection
 490 times 2.5 h, 12 h, and 24 h, see Table 1). Fig. 8a and b show the comparison of the average I_s of compounds (3
 491 samples each) for both filter types, with 2.5h (OA loading of $9.1 \times 10^{-2} \mu\text{g}$) and 24h (OA loading of $1.2 \mu\text{g}$)
 492 collection times. The mass spectra show an overall similar pattern, we observe a non-negligible difference,
 493 especially for the 2.5h samples (Fig. 8a). The log-transformed signals from Quartz and Teflon samples correlate
 494 better for 24-h samples ($R_p = 0.96$, $R_{sp} = 0.95$, Fig. S11d) than for the 2.5-h samples ($R_p = 0.88$, $R_{sp} = 0.87$, Fig.
 495 S11c). In addition, the signal observed for Quartz filter samples is generally slightly lower than for Teflon filter
 496 samples (Fig. 8c, d). Compounds with high Quartz/Teflon-signal ratios are in general semi- or low volatile
 497 compounds (operationally defined as having a $T_{\text{max}} < 60^\circ\text{C}$). These compounds tend to be in the CHO and especially
 498 CHON category and exhibit a higher degree of unsaturation (e.g. $\text{C}_8\text{H}_6\text{O}_3\text{I}^-$, $\text{C}_6\text{H}_5\text{NO}_3\text{I}^-$ and $\text{C}_7\text{H}_6\text{NO}_3\text{I}^-$). They can
 499 be aromatics or their thermal fragmentation products (Liu et al., 2019). Due to the high surface area of the Quartz
 500 filters, semi- or low volatile compounds are more easily adsorbed than on Teflon filters, potentially resulting in
 501 higher positive artefacts. Compounds with low Quartz/Teflon-signal ratios tend to have overall low signal. Despite
 502 the application of a blank determination method that takes instrument backgrounds into account (Method 2b),
 503 higher residuals were still observed for the lower signal compounds, especially for the Teflon filters (as seen also
 504 for the 2.5-h and 0.5-h sample comparison (Fig. 3d). In contrast, compounds with a higher signal tend to be in the
 505 range of Q/T ratios expected based on the observed variability from the reproducibility tests (shown in Fig. 8c and
 506 8d).
 507



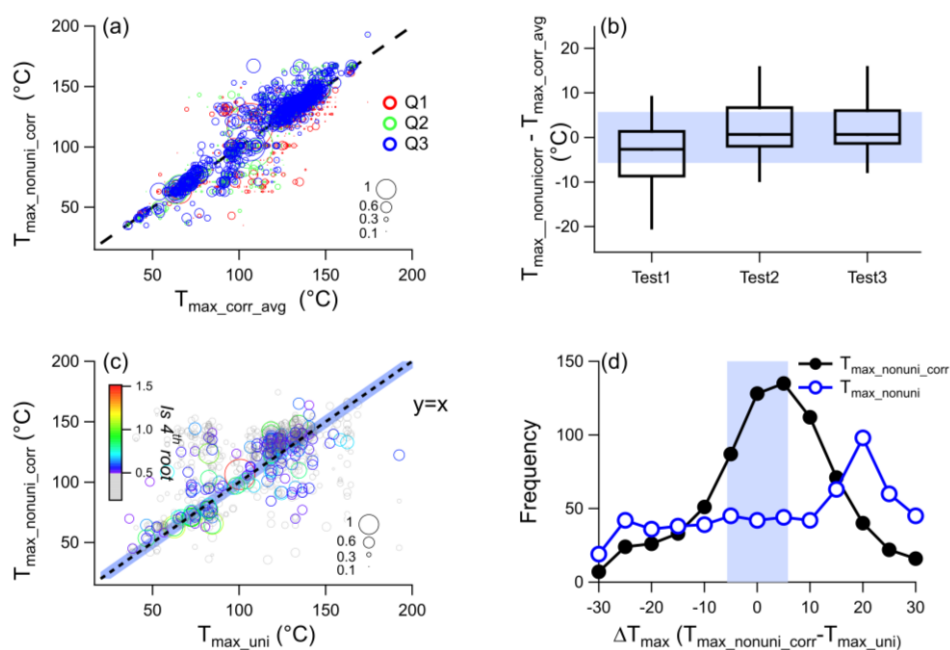
508

509 **Figure 8.** Comparison of the integrated signal intensities of all identified compounds for the Quartz fiber and Teflon filter
 510 samples for (a) 2.5-h samples, and (b) 24-h samples. The size of symbols in (a) and (b) is proportional to the 4th
 511 signal intensity of each compound from the Quartz filter. Frequency distribution (number of compounds) per signal ratio of
 512 Quartz/Teflon for all compounds (green bars), and high-signal compounds (highest 25% signal compounds) only (purple lines)
 513 for 2.5-h samples (c), and 24-h samples (d). The bars in (c) and (d) are colored by the average of the 4th root of the signal
 514 intensity of the Quartz filter. The blue shaded area in each panel represents the possible distribution of I_s ratios of
 515 Quartz/Teflon from the relative errors from the duplicate tests of 2.5-h (25% for Quartz and 31% for Teflon) and 24-h (9%
 516 for Quartz and 18% for Teflon) samples. The upper and lower limits for the 2.5-h Quartz/Teflon I_s ratios were calculated as
 517 $(1+25\%)/(1-31\%)$ and $(1-25\%)/(1+31\%)$, respectively. The upper and lower limits for the 24-h Quartz/Teflon I_s ratios were
 518 calculated as $(1+9\%)/(1-18\%)$ and $(1-9\%)/(1+18\%)$, respectively.

519 3.7 T_{\max} : Influence of temperature ramping protocol and filter type

520 Non-uniform ramping of the temperature due to reagent ion titration is more likely needed when the FIGAERO-
521 CIMS is run in offline mode compared to online mode, where sampling times and resulting filter mass loadings
522 can be adjusted more easily. We have therefore developed a method (see section 2.2.4) to recover T_{\max} from non-
523 uniform ramping protocols, i.e. to make it comparable to T_{\max} from uniform ramping protocols. Compared to the
524 raw thermograms, the shape of the corrected thermograms is more similar to that of the uniform protocol (Fig. S13
525 and S14), since the thermograms were re-gridded to the same temperature intervals (3 °C).

526 Firstly, we tested the variation of T_{\max} from the three duplicate tests of the Quartz filters using the non-uniform
527 ramping protocol and thermogram correction (Fig. 9a). After correction, the corrected T_{\max} ($T_{\max_nonuni_corr}$) from
528 individual tests was highly correlated with their average ($T_{\max_corr_avg}$, $R_p = 0.87\text{--}0.93$). The median value of the
529 difference between $T_{\max_nonuni_corr}$ of duplicate tests and their average for all compounds ranges from $-2.7\text{--}0.7$ °C
530 (shown in Fig.9b). The majority of compounds (52%–70%) have a T_{\max} difference within 5 °C, close to the value
531 reported in previously ($\sim 2^\circ\text{C}$, (Lopez-Hilfiker et al., 2014)). The median standard deviation of the difference
532 between the corrected T_{\max} of individual tests ($T_{\max_nonuni_corr}$) and their average ($T_{\max_corr_avg}$) from all compounds
533 is 5.7 °C, which is defined as the variation of T_{\max} for duplicate tests.



534

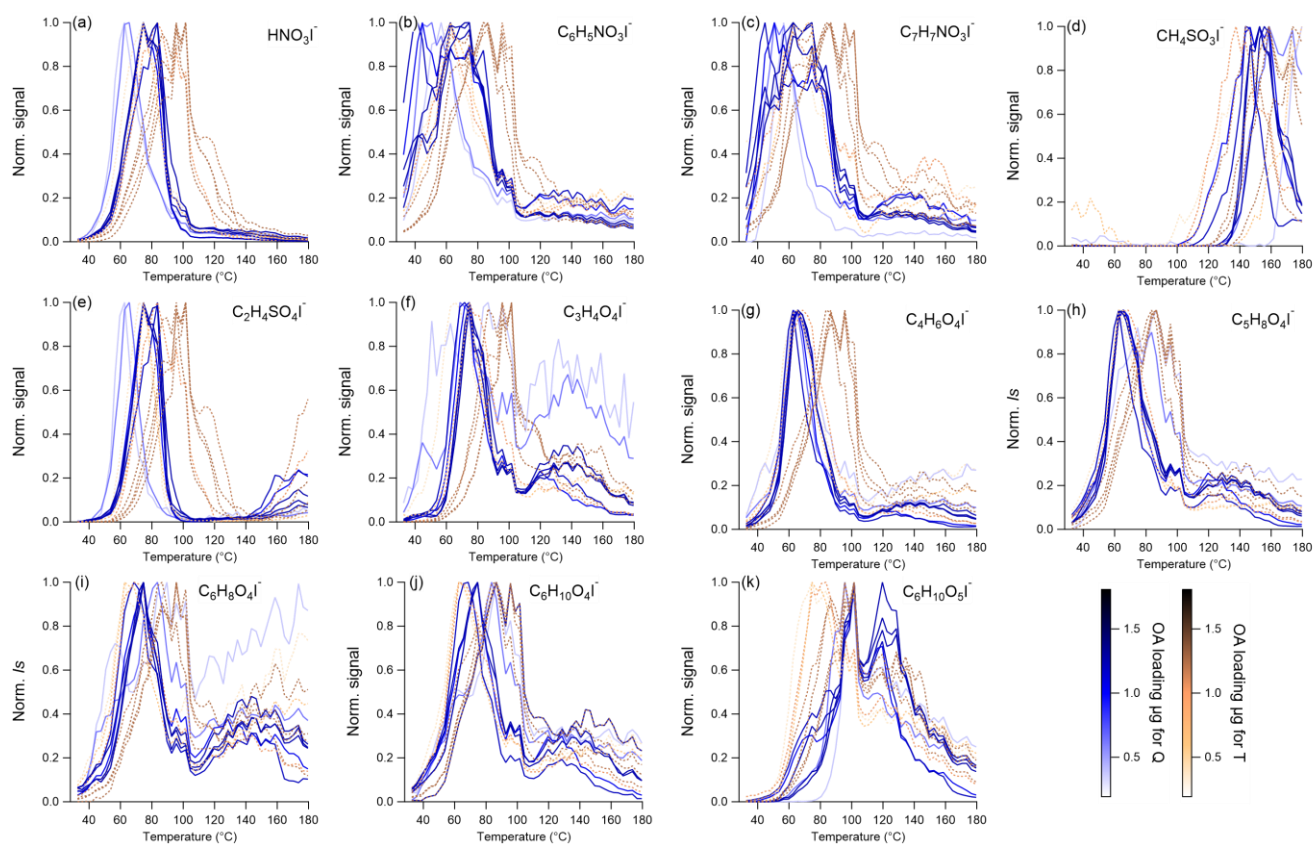
535 **Figure 9.** (a) Comparison of $T_{\max_nonuni_corr}$ from the 3 duplicate tests and their average ($T_{\max_corr_avg}$), (b) distribution of the
536 difference between the 3 triplicate tests and the $T_{\max_corr_avg}$, (c) comparison of T_{\max} from the corrected non-uniform ramping
537 and uniform ramping protocol (T_{\max_uni}), (d) histogram of ΔT_{\max} between T_{\max} from the uniform ramping protocol (T_{\max_uni})
538 and non-uniform with ($T_{\max_nonuni_corr}$)/without (T_{\max_nonuni}) correction. The size of symbols in (a) and (b) is proportional to the
539 4th root of the integrated signal intensity. The 4th root of the signal intensity <0.5 is shown in grey. The uniform ramping
540 protocol test and 3 duplicate non-uniform ramping protocol tests were conducted for the same 24-h Quartz filter (Nov 23 to
541 24). The shaded area in (b), (c), and (d) represents T_{\max} variation ($\pm 5.7^\circ\text{C}$) from the duplicate tests.

542 We take the uniform sampling protocol (see Fig. 1d) as the basis since this is the commonly used protocol for
543 FIGAERO-CIMS in online mode. The comparison of T_{\max} from the corrected non-uniform and the uniform
544 ramping protocols is shown in Fig. 9c. Generally, after correction for the non-uniform ramping, the Pearson
545 correlation coefficient of $T_{\max_nonuni_corr}$ and T_{\max_uni} is higher ($R_p = 0.60$) compared to the uncorrected ones with
546 the uniform protocol ($R_p = 0.20$, T_{\max_nonuni} vs T_{\max_uni}). The correlation coefficients were even higher (0.72 and
547 0.84) for the 400 and 100 compounds with the highest signal intensity. In Fig. 9d we plot the frequency distribution

548 of the differences between the corrected T_{\max} ($T_{\max_nonuni_corr}$) and T_{\max} from the uniform protocol (T_{\max_uni}) for each
 549 CHOX compound in the spectrum. For 73% of the compounds, the difference in T_{\max} between the two ramping
 550 protocols lies between -15 and 15 °C, and 41 % of compounds exhibit a difference of 0 ± 5 °C.

551 In the next step, we compared the volatility derived from T_{\max} for Quartz fiber and Teflon filters. We selected a
 552 number of inorganic and organic compounds, based on their high average signals for the whole sampling period,
 553 for comparison of thermograms from 12-h and 24-h Teflon and Quartz filters sampled in parallel (Table S1, Fig.
 554 10). Compounds include HNO_3I^- , CHON ($\text{C}_6\text{H}_5\text{NO}_3\text{I}^-$, $\text{C}_7\text{H}_7\text{NO}_3\text{I}^-$) and CHOS ($\text{CH}_4\text{SO}_3\text{I}^-$, $\text{C}_2\text{H}_4\text{SO}_4\text{I}^-$) compounds
 555 as well as CHO compounds with $C_{\text{num}} \geq 3$ ($\text{C}_3\text{H}_4\text{O}_4\text{I}^-$, $\text{C}_4\text{H}_6\text{O}_4\text{I}^-$, $\text{C}_5\text{H}_8\text{O}_4\text{I}^-$, $\text{C}_6\text{H}_8\text{O}_4\text{I}^-$, $\text{C}_6\text{H}_{10}\text{O}_4\text{I}^-$, $\text{C}_6\text{H}_{10}\text{O}_5\text{I}^-$).
 556 Compounds with $C_{\text{num}} < 3$ (e.g. $\text{CH}_2\text{O}_2\text{I}^-$) were excluded due to possible gas-phase interference and more likely
 557 influenced by thermal decomposition. Some compounds exhibited similar thermogram shapes for the two types of
 558 filters, such as $\text{C}_6\text{H}_{10}\text{O}_5\text{I}^-$ and $\text{CH}_4\text{SO}_3\text{I}^-$, while for some other species, the thermograms were different. Taking
 559 $\text{C}_3\text{H}_4\text{O}_4\text{I}^-$ as an example, a bimodal thermogram shape with peaks around 100 °C and 150 °C was observed for the
 560 Quartz filter, while only a unimodal peak around 90 °C was observed for the Teflon filter. The different
 561 thermogram shapes of individual compounds for the different filter types might warrant further investigation with
 562 a focus on the role of filter type properties (such as pore size, thickness, absorption, and hydrophobic/hydrophilic
 563 properties).

564



565

566 **Figure 10.** Normalized thermograms for Teflon (T, dashed lines) and Quartz (Q, solid lines) filters of, (a) HNO_3I^- , (b)
 567 $\text{C}_6\text{H}_5\text{NO}_3\text{I}^-$, (c) $\text{C}_7\text{H}_7\text{NO}_3\text{I}^-$, (d) $\text{CH}_4\text{SO}_3\text{I}^-$, (e) $\text{C}_2\text{H}_4\text{SO}_4\text{I}^-$, (f) $\text{C}_3\text{H}_4\text{O}_4\text{I}^-$, (g) $\text{C}_4\text{H}_6\text{O}_4\text{I}^-$, (h) $\text{C}_5\text{H}_8\text{O}_4\text{I}^-$, (i) $\text{C}_6\text{H}_8\text{O}_4\text{I}^-$, (j) $\text{C}_6\text{H}_{10}\text{O}_4\text{I}^-$,
 568 (k) $\text{C}_6\text{H}_{10}\text{O}_5\text{I}^-$. The thermograms were first corrected (section 2.2.4) and then normalized to signals in T_{\max} and colored by the
 569 OA mass loading. The sampling information of the thermograms presented here is listed in Table S1.

570 In addition, we found that compounds with higher mass loadings appeared to have a higher T_{\max} (e.g. $C_2H_4SO_4I^-$
571 and $C_7H_7NO_3I^-$, shown in Fig 10), consistent with previous findings using Teflon filters (Huang et al., 2018;
572 Ylisirniö et al., 2021). The variability in T_{\max} induced by varying PM loadings is within 5°C for 29% of compounds,
573 and within 15°C for 54% of all compounds for Quartz filters, and 35% and 57% of compounds, respectively, for
574 Teflon samples. The higher T_{\max} variation for different OA loading samples compared to the duplicate samples
575 ($\pm 5.7^\circ C$, Fig.9 b) is likely caused by other factors, such as particle viscosity, the particles on the filter, and/or mass
576 loadings on the filter (Huang et al., 2018; Ylisirniö et al., 2021; Wu et al., 2021; Graham et al., 2022). The T_{\max}
577 variation due to filter type ($R_p=0.27$) is much larger than the one induced by filter loadings. Thus, the direct
578 comparison of T_{\max} between Quartz and Teflon filters is not feasible, warranting further research.

579 4. Discussion

580 This study introduces methods and assesses the performance of using the FIGAERO-CIMS in offline mode, i.e.
581 to analyze particulate matter collected temporally and locally distant from the instrument on filter samples (Quartz
582 and Teflon). Such an approach greatly enhances the capabilities of the FIGAERO-CIMS for analyzing atmospheric
583 samples, as it enables the probing of the air at locations where and on occasions when *in-situ* deployments are
584 difficult.

585 Due to the difficulties in background determination for offline FIGAERO-CIMS, in this study, we propose
586 different background determination methods, which were further assessed by the comparison between samples
587 from 5 different 0.5-h samples and a 2.5-h sample collected in parallel. We applied non-uniform temperature
588 ramping to avoid reagent ion titration and a background scaling method taking interference of variable instrument
589 backgrounds into account. In general, the offline FIGAERO-CIMS approach using the methods presented in this
590 study can be used for providing OA composition information with typical offline sampling times (e.g. 12h and
591 24h) samples: (1) the reproducibility of integrated signal intensity is within $\pm 20\%$ for both filter types (18% for
592 Teflon and 9% for Quartz), (2) detected signals respond linearly to changes in the samples' mass loadings, (3) the
593 signals of CHOX and SO_3I^- , HNO_3I^- correlated well with corresponding $PM_{2.5}$ chemical component concentrations
594 of OA, SO_4 , and NO_3 measured by ToF-ACSM ($R_p= 0.94$ to 0.95), (4) the log-transformed mass spectra are highly
595 correlated ($R_p>0.9$) between Quartz and Teflon filters for typical offline sampling times (e.g. 12h and 24h), and
596 for high-signal compounds the I_s ratios between Quartz and Teflon filters are generally within reproducibility
597 variation. Overall, this highlights the possibility of using widely available and stored Quartz filters to identify
598 CHOX molecular composition with FIGAERO-CIMS.

599 T_{\max} retrieved from corrected thermograms of desorption with non-uniform ramping protocols are comparable to
600 T_{\max} from uniform ramping protocol for high signal intensity compounds ($R_p = 0.72-0.84$). More than 50% of
601 compounds have T_{\max} values that are reproducible within 5 °C for duplicate tests ($R_p = 0.87-0.93$) of the same
602 sample, and for >50% of compounds, T_{\max} varies within 15 °C for different mass loadings. Yet, T_{\max} is strongly
603 affected by the filter material (Teflon *vs* Quartz) leading to a large discrepancy in T_{\max} between Quartz and Teflon
604 samples ($R_p = 0.27$), hindering direct comparisons and warranting further research.

605 In summary, using FIGAERO-CIMS to analyze offline samples is a useful and simple way to investigate OA
606 molecular composition, but care needs to be taken for T_{\max} analyses. This opens broad applications to study OA
607 molecular composition, sources, and formation processes at several sites simultaneously and in long-term
608 deployments.

609 *Author contributions*

610 JC, KRD, CM, and MK designed the research. JC, FXZ, and WD collected the samples at the BUCT site. JC, CW,
611 SH, KRD, and CM analyzed the samples and interpreted the data. ZY and CQ analyzed the samples collected at

612 the Peking University campus site. CM, KRD, and MK supervised this research. JC, KRD, and CM wrote the
613 manuscript with contributions from all co-authors. All authors have given approval to the final version of this
614 manuscript.

615 *Acknowledgements*

616 The work is supported by the Knut and Alice Wallenberg Foundation (WAF project CLOUDFORM, grant no.
617 2017.0165), the Academy of Finland (Center of Excellence in Atmospheric Sciences, project no. 307331, and
618 PROFi3 funding, 311932, ACCC Flagship 337549), the European Research Council via ATM-GTP (742206),
619 Wihuri Foundation, and the Jane and Aatos Erkkö Foundation. KRD acknowledges support by the SNF mobility
620 grant P2EZP2_181599. The authors also would like to thank Federico Bianchi's kind help and suggestions as well
621 as the effort from all the researchers in the BUCT project to maintain the BUCT site.

622

623 **Reference**

- 624 Bannan, T. J., Le Breton, M., Priestley, M., Worrall, S. D., Bacak, A., Marsden, N. A., Merha, A., Hammes, J.,
625 Hallquist, M., Alfarra, M. R., Krieger, U. K., Reid, J. P., Jayne, J., Robinson, W., McFiggans, G., Coe, H., Percival,
626 C. J., and Topping, D.: A method for extracting calibrated volatility information from the FIGAERO-HR-ToF-
627 CIMS and its application to chamber and field studies, *Atmospheric Measurement Techniques Discussions*, 1-12,
628 10.5194/amt-2018-255, 2018.
- 629 Cai, J., Wu, C., Wang, J., Du, W., Zheng, F., Hakala, S., Fan, X., Chu, B., Yao, L., Feng, Z., Liu, Y., Sun, Y.,
630 Zheng, J., Yan, C., Bianchi, F., Kulmala, M., Mohr, C., and Daellenbach, K. R.: Influence of organic aerosol
631 molecular composition on particle absorptive properties in autumn Beijing, *Atmospheric Chemistry and Physics*,
632 22, 1251-1269, 10.5194/acp-22-1251-2022, 2022.
- 633 Cai, J., Chu, B., Yao, L., Yan, C., Heikkinen, L. M., Zheng, F., Li, C., Fan, X., Zhang, S., Yang, D., Wang, Y.,
634 Kokkonen, T. V., Chan, T., Zhou, Y., Dada, L., Liu, Y., He, H., Paasonen, P., Kujansuu, J. T., Petäjä, T., Mohr,
635 C., Kangasluoma, J., Bianchi, F., Sun, Y., Croteau, P. L., Worsnop, D. R., Kerminen, V.-M., Du, W., Kulmala,
636 M., and Daellenbach, K. R.: Size-segregated particle number and mass concentrations from different emission
637 sources in urban Beijing, *Atmospheric Chemistry and Physics*, 20, 12721-12740, 10.5194/acp-20-12721-2020,
638 2020.
- 639 Cao, L. M., Huang, X. F., Wang, C., Zhu, Q., and He, L. Y.: Characterization of submicron aerosol volatility in
640 the regional atmosphere in Southern China, *Chemosphere*, 236, 124383, 10.1016/j.chemosphere.2019.124383,
641 2019.
- 642 Cappa, C. D., Onasch, T. B., Massoli, P., Worsnop, D. R., Bates, T. S., Cross, E. S., Davidovits, P., Hakala, J.,
643 Hayden, K. L., Jobson, B. T., Kolesar, K. R., Lack, D. A., Lerner, B. M., Li, S.-M., Mellon, D., Nuaaman, I.,
644 Olfert, J. S., Petäjä, T., Quinn, P. K., Song, C., Subramanian, R., Williams, E. J., and Zaveri, R. A.: Radiative
645 Absorption Enhancements Due to the Mixing State of Atmospheric Black Carbon, *Science*, 337, 1078-1081, 2012.
- 646 Cheng, Y., He, K. B., Duan, F. K., Zheng, M., Ma, Y. L., and Tan, J. H.: Measurement of semivolatile
647 carbonaceous aerosols and its implications: a review, *Environ Int*, 35, 674-681, 10.1016/j.envint.2008.11.007,
648 2009.
- 649 Daellenbach, K. R., Uzu, G., Jiang, J., Cassagnes, L. E., Leni, Z., Vlachou, A., Stefenelli, G., Canonaco, F., Weber,
650 S., Segers, A., Kuenen, J. J. P., Schaap, M., Favez, O., Albinet, A., Aksoyoglu, S., Dommen, J., Baltensperger, U.,
651 Geiser, M., El Haddad, I., Jaffrezo, J. L., and Prevot, A. S. H.: Sources of particulate-matter air pollution and its
652 oxidative potential in Europe, *Nature*, 587, 414-419, 10.1038/s41586-020-2902-8, 2020.
- 653 Fan, X., Cai, J., Yan, C., Zhao, J., Guo, Y., Li, C., Dällenbach, K. R., Zheng, F., Lin, Z., Chu, B., Wang, Y., Dada,
654 L., Zha, Q., Du, W., Kontkanen, J., Kurtén, T., Iyer, S., Kujansuu, J. T., Petäjä, T., Worsnop, D. R., Kerminen,
655 V.-M., Liu, Y., Bianchi, F., Tham, Y. J., Yao, L., and Kulmala, M.: Atmospheric gaseous hydrochloric and

656 hydrobromic acid in urban Beijing, China: detection, source identification and potential atmospheric impacts,
657 Atmospheric Chemistry and Physics, 21, 11437-11452, 10.5194/acp-21-11437-2021, 2021.

658 Farmer, D. K., Vance, M. E., Abbatt, J. P. D., Abeleira, A., Alves, M. R., Arata, C., Boedicker, E., Bourne, S.,
659 Cardoso-Saldana, F., Corsi, R., DeCarlo, P. F., Goldstein, A. H., Grassian, V. H., Hildebrandt Ruiz, L., Jimenez,
660 J. L., Kahan, T. F., Katz, E. F., Mattila, J. M., Nazaroff, W. W., Novoselac, A., O'Brien, R. E., Or, V. W., Patel,
661 S., Sankhyan, S., Stevens, P. S., Tian, Y., Wade, M., Wang, C., Zhou, S., and Zhou, Y.: Overview of HOMEChem:
662 House Observations of Microbial and Environmental Chemistry, Environ Sci Process Impacts, 21, 1280-1300,
663 10.1039/c9em00228f, 2019.

664 Graham, E. L., Wu, C., Bell, D. M., Bertrand, A., Haslett, S. L., Baltensperger, U., El Haddad, I., Krejci, R.,
665 Riipinen, I., and Mohr, C., 10.5194/egusphere-2022-1043, 2022.

666 Guo, Y., Yan, C., Li, C., Ma, W., Feng, Z., Zhou, Y., Lin, Z., Dada, L., Stolzenburg, D., Yin, R., Kontkanen, J.,
667 Daellenbach, K. R., Kangasluoma, J., Yao, L., Chu, B., Wang, Y., Cai, R., Bianchi, F., Liu, Y., and Kulmala, M.:
668 Formation of nighttime sulfuric acid from the ozonolysis of alkenes in Beijing, Atmospheric Chemistry and
669 Physics, 21, 5499-5511, 10.5194/acp-21-5499-2021, 2021.

670 Gustafson, K. E. and Dickhut, R. M.: Particle/Gas Concentrations and Distributions of PAHs in the Atmosphere
671 of Southern Chesapeake Bay, Environmental Science & Technology, 31, 140-147, 10.1021/es9602197, 1997.

672 Huang, R. J., Zhang, Y., Bozzetti, C., Ho, K. F., Cao, J. J., Han, Y., Daellenbach, K. R., Slowik, J. G., Platt, S. M.,
673 Canonaco, F., Zotter, P., Wolf, R., Pieber, S. M., Brun, E. A., Crippa, M., Ciarelli, G., Piazzalunga, A.,
674 Schwikowski, M., Abbazade, G., Schnelle-Kreis, J., Zimmermann, R., An, Z., Szidat, S., Baltensperger, U., El
675 Haddad, I., and Prevot, A. S.: High secondary aerosol contribution to particulate pollution during haze events in
676 China, Nature, 514, 218-222, 10.1038/nature13774, 2014.

677 Huang, W., Saathoff, H., Shen, X., Ramisetty, R., Leisner, T., and Mohr, C.: Seasonal characteristics of organic
678 aerosol chemical composition and volatility in Stuttgart, Germany, Atmospheric Chemistry and Physics, 19,
679 11687-11700, 10.5194/acp-19-11687-2019, 2019a.

680 Huang, W., Saathoff, H., Shen, X., Ramisetty, R., Leisner, T., and Mohr, C.: Chemical Characterization of Highly
681 Functionalized Organonitrates Contributing to Night-Time Organic Aerosol Mass Loadings and Particle Growth,
682 Environ Sci Technol, 53, 1165-1174, 10.1021/acs.est.8b05826, 2019b.

683 Huang, W., Saathoff, H., Pajunoja, A., Shen, X., Naumann, K.-H., Wagner, R., Virtanen, A., Leisner, T., and
684 Mohr, C.: α -Pinene secondary organic aerosol at low temperature: chemical composition and
685 implications for particle viscosity, Atmospheric Chemistry and Physics, 18, 2883-2898, 10.5194/acp-18-2883-
686 2018, 2018.

687 Jia, Y., Rahn, K. A., He, K., Wen, T., and Wang, Y.: A novel technique for quantifying the regional component
688 of urban aerosol solely from its sawtooth cycles, Journal of Geophysical Research, 113, 10.1029/2008jd010389,
689 2008.

690 Kontkanen, J., Deng, C., Fu, Y., Dada, L., Zhou, Y., Cai, J., Dällenbach, K. R., Hakala, S., Kokkonen, T. V., Lin,
691 Z., Liu, Y., Wang, Y., Yan, C., Petäjä, T., Jiang, J., Kulmala, M., and Paasonen, P., 10.5194/acp-2020-215, 2020.

692 Koss, A. R., Sekimoto, K., Gilman, J. B., Selimovic, V., Coggon, M. M., Zarzana, K. J., Yuan, B., Lerner, B. M.,
693 Brown, S. S., Jimenez, J. L., Krechmer, J., Roberts, J. M., Warneke, C., Yokelson, R. J., and de Gouw, J.: Non-
694 methane organic gas emissions from biomass burning: identification, quantification, and emission factors from
695 PTR-ToF during the FIREX 2016 laboratory experiment, Atmospheric Chemistry and Physics, 18, 3299-3319,
696 10.5194/acp-18-3299-2018, 2018.

697 Kulmala, M., Dada, L., Daellenbach, K. R., Yan, C., Stolzenburg, D., Kontkanen, J., Ezhova, E., Hakala, S.,
698 Tuovinen, S., Kokkonen, T. V., Kurppa, M., Cai, R., Zhou, Y., Yin, R., Baalbaki, R., Chan, T., Chu, B., Deng, C.,
699 Fu, Y., Ge, M., He, H., Heikkinen, L., Junninen, H., Liu, Y., Lu, Y., Nie, W., Rusanen, A., Vakkari, V., Wang, Y.,
700 Yang, G., Yao, L., Zheng, J., Kujansuu, J., Kangasluoma, J., Petaja, T., Paasonen, P., Jarvi, L., Worsnop, D., Ding,
701 A., Liu, Y., Wang, L., Jiang, J., Bianchi, F., and Kerminen, V. M.: Is reducing new particle formation a plausible
702 solution to mitigate particulate air pollution in Beijing and other Chinese megacities?, Faraday Discuss, 226, 334-
703 347, 10.1039/d0fd00078g, 2021.

704 Le Breton, M., Psychoudaki, M., Hallquist, M., Watne, Å. K., Lutz, A., and Hallquist, Å. M.: Application of a
705 FIGAERO ToF CIMS for on-line characterization of real-world fresh and aged particle emissions from buses,
706 Aerosol Science and Technology, 53, 244-259, 10.1080/02786826.2019.1566592, 2019.

707 Lee, B. H., Lopez-Hilfiker, F. D., amp, apos, Ambro, E. L., Zhou, P., Boy, M., Petäjä, T., Hao, L., Virtanen, A.,
708 and Thornton, J. A.: Semi-volatile and highly oxygenated gaseous and particulate organic compounds observed
709 above a boreal forest canopy, *Atmospheric Chemistry and Physics*, 18, 11547-11562, 10.5194/acp-18-11547-2018,
710 2018.

711 Lee, B. H., Mohr, C., Lopez-Hilfiker, F. D., Lutz, A., Hallquist, M., Lee, L., Romer, P., Cohen, R. C., Iyer, S.,
712 Kurten, T., Hu, W., Day, D. A., Campuzano-Jost, P., Jimenez, J. L., Xu, L., Ng, N. L., Guo, H., Weber, R. J., Wild,
713 R. J., Brown, S. S., Koss, A., de Gouw, J., Olson, K., Goldstein, A. H., Seco, R., Kim, S., McAvey, K., Shepson,
714 P. B., Starn, T., Baumann, K., Edgerton, E. S., Liu, J., Shilling, J. E., Miller, D. O., Brune, W., Schobesberger, S.,
715 D'Ambro, E. L., and Thornton, J. A.: Highly functionalized organic nitrates in the southeast United States:
716 Contribution to secondary organic aerosol and reactive nitrogen budgets, *Proc Natl Acad Sci U S A*, 113, 1516-
717 1521, 10.1073/pnas.1508108113, 2016.

718 Liu, L., Rao, Z., Wang, Y., Arandiyan, H., Gong, J., Liang, M., and Guo, F.: Characteristics and Health Risk
719 Assessment of Semi-Volatile Organic Contaminants in Rural Pond Water of Hebei Province, *Int J Environ Res*
720 *Public Health*, 16, 10.3390/ijerph16224481, 2019.

721 Liu, Q., Baumgartner, J., Zhang, Y., and Schauer, J. J.: Source apportionment of Beijing air pollution during a
722 severe winter haze event and associated pro-inflammatory responses in lung epithelial cells, *Atmospheric*
723 *Environment*, 126, 28-35, <https://doi.org/10.1016/j.atmosenv.2015.11.031>, 2016.

724 Liu, Y., Zhang, Y., Lian, C., Yan, C., Feng, Z., Zheng, F., Fan, X., Chen, Y., Wang, W., Chu, B., Wang, Y., Cai,
725 J., Du, W., Daellenbach, K. R., Kangasluoma, J., Bianchi, F., Kujansuu, J., Petäjä, T., Wang, X., Hu, B., Wang,
726 Y., Ge, M., He, H., and Kulmala, M.: The promotion effect of nitrous acid on aerosol formation in wintertime in
727 Beijing: the possible contribution of traffic-related emissions, *Atmospheric Chemistry and Physics*, 20, 13023-
728 13040, 10.5194/acp-20-13023-2020, 2020.

729 Lopez-Hilfiker, F. D., Pospisilova, V., Huang, W., Kalberer, M., Mohr, C., Stefenelli, G., Thornton, J. A.,
730 Baltensperger, U., Prevot, A. S. H., and Slowik, J. G.: An extractive electrospray ionization time-of-flight mass
731 spectrometer (EESI-TOF) for online measurement of atmospheric aerosol particles, *Atmospheric Measurement*
732 *Techniques*, 12, 4867-4886, 10.5194/amt-12-4867-2019, 2019.

733 Lopez-Hilfiker, F. D., Mohr, C., Ehn, M., Rubach, F., Kleist, E., Wildt, J., Mentel, T. F., Lutz, A., Hallquist, M.,
734 Worsnop, D., and Thornton, J. A.: A novel method for online analysis of gas and particle composition: description
735 and evaluation of a Filter Inlet for Gases and AEROSols (FIGAERO), *Atmospheric Measurement Techniques*, 7,
736 983-1001, 10.5194/amt-7-983-2014, 2014.

737 Lopez-Hilfiker, F. D., Mohr, C., D'Ambro, E. L., Lutz, A., Riedel, T. P., Gaston, C. J., Iyer, S., Zhang, Z., Gold,
738 A., Surratt, J. D., Lee, B. H., Kurten, T., Hu, W. W., Jimenez, J., Hallquist, M., and Thornton, J. A.: Molecular
739 Composition and Volatility of Organic Aerosol in the Southeastern U.S.: Implications for IEPOX Derived SOA,
740 *Environ Sci Technol*, 50, 2200-2209, 10.1021/acs.est.5b04769, 2016.

741 Masoud, C. G., Li, Y., Wang, D. S., Katz, E. F., DeCarlo, P. F., Farmer, D. K., Vance, M. E., Shiraiwa, M., and
742 Hildebrandt Ruiz, L.: Molecular composition and gas-particle partitioning of indoor cooking aerosol: Insights from
743 a FIGAERO-CIMS and kinetic aerosol modeling, *Aerosol Science and Technology*, 56, 1156-1173,
744 10.1080/02786826.2022.2133593, 2022.

745 Mohr, C., Thornton, J. A., Heitto, A., Lopez-Hilfiker, F. D., Lutz, A., Riipinen, I., Hong, J., Donahue, N. M.,
746 Hallquist, M., Petaja, T., Kulmala, M., and Yli-Juuti, T.: Molecular identification of organic vapors driving
747 atmospheric nanoparticle growth, *Nat Commun*, 10, 4442, 10.1038/s41467-019-12473-2, 2019.

748 Nozriere, B., Kalberer, M., Claeys, M., Allan, J., D'Anna, B., Decesari, S., Finessi, E., Glasius, M., Grgic, I.,
749 Hamilton, J. F., Hoffmann, T., Iinuma, Y., Jaoui, M., Kahnt, A., Kampf, C. J., Kourtschev, I., Maenhaut, W.,
750 Marsden, N., Saarikoski, S., Schnelle-Kreis, J., Surratt, J. D., Szidat, S., Szmigielski, R., and Wisthaler, A.: The
751 molecular identification of organic compounds in the atmosphere: state of the art and challenges, *Chem Rev*, 115,
752 3919-3983, 10.1021/cr5003485, 2015.

753 Riipinen, I., Yli-Juuti, T., Pierce, J. R., Petäjä, T., Worsnop, D. R., Kulmala, M., and Donahue, N. M.: The
754 contribution of organics to atmospheric nanoparticle growth, *Nature Geoscience*, 5, 453-458, 10.1038/ngeo1499,
755 2012.

756 Schauer, J. J., Kleeman, M. J., Cass, G. R., and Simoneit, B. R. T.: Measurement of Emissions from Air Pollution
757 Sources. 4. C1–C27 Organic Compounds from Cooking with Seed Oils, *Environmental Science & Technology*,
758 36, 567-575, 10.1021/es002053m, 2002.

759 Siegel, K., Zieger, P., Salter, M., Riipinen, I., Ekman, A. M. L., and Mohr, C.: Chemical composition of
760 summertime High Arctic aerosols using chemical ionization mass spectrometry, May 01, 20202020.

761 Siegel, K., Karlsson, L., Zieger, P., Baccarini, A., Schmale, J., Lawler, M., Salter, M., Leck, C., Ekman, A. M. L.,
762 Riipinen, I., and Mohr, C.: Insights into the molecular composition of semi-volatile aerosols in the summertime
763 central Arctic Ocean using FIGAERO-CIMS, *Environmental Science: Atmospheres*, 10.1039/d0ea00023j, 2021.

764 Tao, J., Zhang, L., Cao, J., and Zhang, R.: A review of current knowledge concerning PM_{2.5}
765 chemical composition, aerosol optical properties and their relationships across China, *Atmospheric Chemistry and
766 Physics*, 17, 9485-9518, 10.5194/acp-17-9485-2017, 2017.

767 Thornton, J. A., Mohr, C., Schobesberger, S., D'Ambro, E. L., Lee, B. H., and Lopez-Hilfiker, F. D.: Evaluating
768 Organic Aerosol Sources and Evolution with a Combined Molecular Composition and Volatility Framework Using
769 the Filter Inlet for Gases and Aerosols (FIGAERO), *Accounts of Chemical Research*, 53, 1415-1426,
770 10.1021/acs.accounts.0c00259, 2020.

771 Turpin, B. J. and Lim, H.-J.: Species Contributions to PM_{2.5} Mass Concentrations: Revisiting Common
772 Assumptions for Estimating Organic Mass, *Aerosol Science and Technology*, 35, 602-610,
773 10.1080/02786820119445, 2001.

774 Turpin, B. J., Saxena, P., and Andrews, E.: Measuring and simulating particulate organics in the atmosphere:
775 problems and prospects, *Atmospheric Environment*, 34, 2983-3013, [https://doi.org/10.1016/S1352-
776 2310\(99\)00501-4](https://doi.org/10.1016/S1352-2310(99)00501-4), 2000.

777 Wang, J. M., Jeong, C.-H., Hilker, N., Shairsingh, K. K., Healy, R. M., Sofowote, U., Debosz, J., Su, Y.,
778 McGaughey, M., Doerksen, G., Munoz, T., White, L., Herod, D., and Evans, G. J.: Near-Road Air Pollutant
779 Measurements: Accounting for Inter-Site Variability Using Emission Factors, *Environmental Science &
780 Technology*, 52, 9495-9504, 10.1021/acs.est.8b01914, 2018.

781 Watson, J. G. and Chow, J. C.: Comparison and evaluation of in situ and filter carbon measurements at the Fresno
782 Supersite, *Journal of Geophysical Research: Atmospheres*, 107, ICC 3-1-ICC 3-15, 10.1029/2001jd000573, 2002.

783 Wu, C., Bell, D. M., Graham, E. L., Haslett, S., Riipinen, I., Baltensperger, U., Bertrand, A., Giannoukos, S.,
784 Schoonbaert, J., El Haddad, I., Prevot, A. S. H., Huang, W., and Mohr, C.: Photolytically induced changes in
785 composition and volatility of biogenic secondary organic aerosol from nitrate radical oxidation during night-to-
786 day transition, *Atmospheric Chemistry and Physics*, 21, 14907-14925, 10.5194/acp-21-14907-2021, 2021.

787 Yao, L., Garmash, O., Bianchi, F., Zheng, J., Yan, C., Kontkanen, J., Junninen, H., Mazon, S. B., Ehn, M.,
788 Paasonen, P., Sipila, M., Wang, M. Y., Wang, X. K., Xiao, S., Chen, H. F., Lu, Y. Q., Zhang, B. W., Wang, D. F.,
789 Fu, Q. Y., Geng, F. H., Li, L., Wang, H. L., Qiao, L. P., Yang, X., Chen, J. M., Kerminen, V. M., Petaja, T.,
790 Worsnop, D. R., Kulmala, M., and Wang, L.: Atmospheric new particle formation from sulfuric acid and amines
791 in a Chinese megacity, *Science*, 361, 278+, 10.1126/science.aao4839, 2018.

792 Yao, L., Fan, X., Yan, C., Kurten, T., Daellenbach, K. R., Li, C., Wang, Y., Guo, Y., Dada, L., Rissanen, M. P.,
793 Cai, J., Tham, Y. J., Zha, Q., Zhang, S., Du, W., Yu, M., Zheng, F., Zhou, Y., Kontkanen, J., Chan, T., Shen, J.,
794 Kujansuu, J. T., Kangasluoma, J., Jiang, J., Wang, L., Worsnop, D. R., Petaja, T., Kerminen, V. M., Liu, Y., Chu,
795 B., He, H., Kulmala, M., and Bianchi, F.: Unprecedented Ambient Sulfur Trioxide (SO₃) Detection: Possible
796 Formation Mechanism and Atmospheric Implications, *Environ Sci Technol Lett*, 7, 809-818,
797 10.1021/acs.estlett.0c00615, 2020.

798 Ye, C., Yuan, B., Lin, Y., Wang, Z., Hu, W., Li, T., Chen, W., Wu, C., Wang, C., Huang, S., Qi, J., Wang, B.,
799 Wang, C., Song, W., Wang, X., Zheng, E., Krechmer, J. E., Ye, P., Zhang, Z., Wang, X., Worsnop, D. R., and
800 Shao, M.: Chemical characterization of oxygenated organic compounds in the gas phase and particle phase using
801 iodide CIMS with FIGAERO in urban air, *Atmos. Chem. Phys.*, 21, 8455-8478, 10.5194/acp-21-8455-2021, 2021.

802 Ylisirniö, A., Barreira, L. M. F., Pullinen, I., Buchholz, A., Jayne, J., Krechmer, J. E., Worsnop, D. R., Virtanen,
803 A., and Schobesberger, S.: On the calibration of FIGAERO-ToF-CIMS: importance and impact of calibrant
804 delivery for the particle-phase calibration, *Atmos. Meas. Tech.*, 14, 355-367, 10.5194/amt-14-355-2021, 2021.

805 Zheng, Y., Chen, Q., Cheng, X., Mohr, C., Cai, J., Huang, W., Shrivastava, M., Ye, P., Fu, P., Shi, X., Ge, Y.,
806 Liao, K., Miao, R., Qiu, X., Koenig, T. K., and Chen, S.: Precursors and Pathways Leading to Enhanced Secondary

807 Organic Aerosol Formation during Severe Haze Episodes, Environ Sci Technol, 55, 15680-15693,
808 10.1021/acs.est.1c04255, 2021.

809